

1 **TITLE**

2 “Coordination of peptidoglycan synthesis and outer membrane constriction during *Escherichia coli* cell
3 division”

4

5 **AUTHOR NAMES AND AFFILIATIONS**

6 Andrew N. Gray^{1#}, Alexander J. F. Egan^{2#}, Inge L. van't Veer³, Jolanda Verheul⁴, Alexandre Colavin⁵,
7 Alexandra Koumoutsis⁶, Jacob Biboy², Maarten A. F. Altelaar⁷, Mirjam J. Damen⁷, Kerwyn Casey
8 Huang^{5,8,9}, Jean-Pierre Simorre¹⁰, Eefjan Breukink³, Tanneke den Blaauwen^{4*}, Athanasios Typas^{6*},
9 Carol A. Gross^{1,11*} and Waldemar Vollmer^{2*}

10 [#]These authors contributed equally to this work

11 ¹Department of Microbiology & Immunology, University of California at San Francisco, San Francisco,
12 CA 94158-2517, USA

13 ²Centre for Bacterial Cell Biology, Institute for Cell and Molecular Biosciences, Newcastle University,
14 Richardson Road, Newcastle upon Tyne, NE2 4AX, UK

15 ³Membrane Biochemistry & Biophysics, Bijvoet Centre for Biomolecular Research, University of Utrecht,
16 Padualaan 8, 3584 CH Utrecht, The Netherlands

17 ⁴Bacterial Cell Biology, Swammerdam Institute for Life Sciences, Faculty of Science, University of
18 Amsterdam, Science Park 904, 1098 XH Amsterdam, The Netherlands

19 ⁵Biophysics Program, Stanford University, Stanford, CA 94305, USA

20 ⁶European Molecular Biology Laboratory Heidelberg, Genome Biology Unit, Meyerhofstraße 1, 69117
21 Heidelberg, Germany

22 ⁷Biomolecular Mass Spectrometry and Proteomics, Bijvoet Centre for Biomolecular Research,
23 University of Utrecht, Padualaan 8, 3584 CH Utrecht, The Netherlands

24 ⁸Department of Bioengineering, Stanford University, Stanford, CA 94305, USA

25 ⁹Department of Microbiology and Immunology, Stanford University School of Medicine, Stanford, CA
26 94305, USA

27 ¹⁰Univ. Grenoble Alpes, Institut de Biologie Structurale (IBS), F-38000 Grenoble, France; CEA, DSV,
28 IBS, F-38000 Grenoble, France; and ×CNRS, IBS, F-38000 Grenoble, France

29 ¹¹Department of Cell and Tissue Biology, University of California at San Francisco, San Francisco,
30 California 94158, USA

31

32 ***For correspondence:** Tanneke den Blaauwen, T.denBlaauwen@uva.nl; Athanasios Typas,
33 typas@embl.de; Carol A. Gross, cgrossucsf@gmail.com; Waldemar Vollmer, w.vollmer@ncl.ac.uk

34

35 **Competing interests:** The authors declare that no competing interests exist.

36 **ABSTRACT**

37

38 To maintain cellular structure and integrity during division, Gram-negative bacteria must carefully
39 coordinate constriction of a tripartite cell envelope of inner membrane (IM), peptidoglycan (PG) and
40 outer membrane (OM). It has remained enigmatic how this is accomplished. Here, we show that
41 envelope-spanning machineries of septal PG synthesis (PBP1B-LpoB) and OM constriction (Tol-Pal)
42 are physically and functionally coordinated via YbgF, renamed CpoB (Coordinator of PG synthesis and
43 OM constriction, associated with PBP1B). CpoB localizes to the septum concurrent with PBP1B-LpoB
44 and Tol-Pal at the onset of constriction, interacts with both complexes, and regulates PBP1B activity in
45 response to Tol-Pal energy state. This coordination links PG synthesis with OM invagination and
46 imparts a unique mode of bifunctional PG synthase regulation by selectively modulating PBP1B cross-
47 linking activity. Coordination of the PBP1B and Tol-Pal machines by CpoB is critical for effective PBP1B
48 function *in vivo* and for maintaining cell envelope integrity during division.

49 INTRODUCTION

50

51 Cell shape and osmotic stability are maintained by the stress-bearing peptidoglycan (PG)
52 sacculus (cell wall) in nearly all bacteria (Vollmer *et al.*, 2008). The sacculus, a continuous mesh-like
53 structure of glycan strands cross-linked by short peptides, encases the inner (cytoplasmic) membrane
54 (IM) and is essential for viability. Several prominent classes of antibiotics (e.g., β -lactams and
55 glycopeptides) inhibit PG synthesis, causing lysis and cell death (Schneider and Sahl, 2010). In Gram-
56 negative bacteria, the outer membrane (OM), an asymmetric bilayer of phospholipids and
57 lipopolysaccharides, surrounds the mostly single-layered sacculus (Gan *et al.*, 2008) and forms a vital
58 permeability barrier (Nikaido, 2003). Covalent and non-covalent interactions between abundant OM
59 proteins (Lpp, Pal, OmpA) and PG tether the OM to the sacculus, maintaining OM stability (Hantke and
60 Braun, 1973, Parsons *et al.*, 2006). Together, the IM, PG, and OM comprise the tripartite Gram-
61 negative cell envelope. Bacteria must synchronize growth and division of these layers, as imbalanced
62 growth could lead to breaches that compromise the permeability barrier and even the structural integrity
63 of the cell. However, we do not yet understand the mechanisms that accomplish this synchronization.

64

65 Coordinating growth across the layers of the Gram-negative bacterial cell envelope is complex,
66 particularly since all energy and precursors for assembling and constricting these layers must come
67 from the cytoplasm. To overcome this challenge, bacteria utilize IM-associated multicomponent

68 machineries that span the entire envelope. Two machineries, organized by distinct cytoskeletal
69 elements, assemble and disassemble in a cell-cycle-regulated manner and mediate different phases of
70 sacculus growth (Typas *et al.*, 2012): 1) the cell elongation machinery (elongasome), organized by the
71 actin homolog MreB, mediates lateral PG synthesis along the length of the cell, and 2) the cell division
72 machinery (divisome), organized by the tubulin homolog FtsZ, mediates new pole synthesis at the
73 septum (Egan and Vollmer, 2013). These complex machineries are comprised of structural and
74 regulatory subunits, components with distinct functions (e.g., DNA segregation, PG precursor synthesis
75 and transport), and PG biosynthetic and modifying enzymes.

76

77 Sacculus growth is orchestrated by a repertoire of PG synthases, including glycosyltransferases
78 (GTases) that polymerize glycan strands from the precursor saccharide moiety lipid II, transpeptidases
79 (TPases) that cross-link peptides between adjacent glycan strands, and bifunctional PG synthases that
80 carry out both activities (Typas *et al.*, 2012). The two *E. coli* monofunctional TPases, PBP2 and PBP3,
81 are essential subunits of the elongasome and the divisome, respectively. Likewise, the two major
82 bifunctional PG synthases, PBP1A and PBP1B, participate predominantly in elongation and division,
83 respectively (Banzhaf *et al.*, 2012, Bertsche *et al.*, 2006, Typas *et al.*, 2010). However, in contrast to the
84 monofunctional TPases, which are dedicated to their respective roles, the bifunctional synthases can
85 partially substitute for each other, enabling cells to survive with only one of them (Yousif *et al.*, 1985).
86 These IM-localized bifunctional synthases have obligate cognate regulatory OM lipoproteins, LpoA and

87 LpoB, which are required for activity *in vivo* (Typas *et al.*, 2010, Paradis-Bleau *et al.*, 2010). The Lpo
88 activators span most of the periplasm (~210 Å in width (Matias *et al.*, 2003)) and traverse the sacculus
89 (~40-60 Å pore size (Demchick and Koch, 1996, Vazquez-Laslop *et al.*, 2001)) to interact with their
90 partner PBPs (Jean *et al.*, 2014, Egan *et al.*, 2014), forming trans-envelope PG synthase complexes.

91

92 Electron microscopy studies first indicated that distances between the OM, PG and IM remain
93 remarkably consistent throughout cell division, providing an early indication that envelope constriction
94 processes occur in close proximity to each other and are tightly coordinated (Bi and Lutkenhaus, 1991,
95 Fung *et al.*, 1978, Weigand *et al.*, 1976, MacAlister *et al.*, 1987). It is now clear that IM constriction, PG
96 synthesis, and subsequent PG hydrolysis to separate daughter cells (septal cleavage) are coordinated
97 via the divisome. FtsZ forms a ring-like structure in the cytoplasm that provides the membrane
98 contractile force (Osawa *et al.*, 2009), and together with FtsA (Loose and Mitchison, 2014, Szwedziak
99 *et al.*, 2014, Szwedziak *et al.*, 2012, Osawa and Erickson, 2013) serves as a scaffold for divisome
100 assembly, including recruitment of PG synthases and hydrolases (Egan and Vollmer, 2013). Septal PG
101 synthesis, orchestrated by PBP3 and PBP1B (Bertsche *et al.*, 2006), occurs at the front of the inward-
102 moving septum, adjacent to the invaginating IM. Septal cleavage, controlled by tightly regulated
103 periplasmic amidases (Heidrich *et al.*, 2001, Uehara *et al.*, 2010), follows closely after synthesis and
104 adjacent to the invaginating OM. Both topological constraints and regulatory input from IM and/or OM
105 proteins ensure tight spatial regulation of septal cleavage (Uehara *et al.*, 2010, Yang *et al.*, 2011).

106

107 OM constriction is promoted by the membrane-spanning Tol-Pal complex, which localizes to
108 mid-cell during the later stages of cell division in a divisome-dependent manner (Gerding *et al.*, 2007).
109 Comprised of IM proteins TolQ, TolR, and TolA, periplasmic TolB, and OM lipoprotein Pal, the Tol-Pal
110 machine has been proposed to harness proton motive force (PMF) via TolQR to energize TolA,
111 inducing it to adopt an extended conformation and interact with TolB and/or Pal (Germon *et al.*, 2001,
112 Cascales *et al.*, 2000, Lloubes *et al.*, 2001). Cycles of interaction and release are then thought to
113 promote OM invagination (Gerding *et al.*, 2007). Loss of Tol-Pal function results in delayed OM
114 constriction and defects in OM integrity, leading to OM blebbing, periplasmic leakage, and pleiotropic
115 drug and stress sensitivities (Gerding *et al.*, 2007, Bernadac *et al.*, 1998, Cascales *et al.*, 2002).
116 Whether Tol-Pal-mediated OM constriction, occurring at the back of the inwardly progressing envelope,
117 is actively coordinated with PG septal synthesis, occurring at the front, remains completely unknown.

118

119 We previously identified a genetic link between PBP1B-LpoB and Tol-Pal (Typas *et al.*, 2010).
120 Here, we report that physical and functional coordination of the two machineries is required to properly
121 synchronize PG synthesis and OM constriction during cell division. We implicate YbgF, previously of
122 unknown function, in mediating this coordination, and therefore name it CpoB, or Coordinator of PG
123 synthesis and OM constriction, associated with PBP1B. We show that CpoB, PBP1B-LpoB, and Tol-Pal
124 localize concurrently to the septum during cell division, and interact to form a higher-order complex that

125 spatially links PG synthesis and OM invagination. These physical interactions are dynamic and possess
126 functional correlates, allowing direct regulation of PBP1B activity in response to Tol-Pal assembly and
127 cycles of PMF utilization. CpoB is required for proper PBP1B function *in vivo*, and loss of CpoB-
128 mediated coordination between PBP1B and Tol-Pal leads to defects in OM integrity, illustrating the
129 importance of mechanisms that ensure coordination of cell division processes across the envelope.

130 RESULTS

131

132 Chemical sensitivities, genetic interactions, and physical association implicate CpoB, an 133 auxiliary Tol-Pal-associated protein, in PBP1B function

134 To identify novel regulators of PG synthesis during cell division, we queried the *E. coli* chemical
135 genomics database (Nichols *et al.*, 2011) to identify deletion strains whose growth responses closely
136 resembled those of a strain lacking PBP1B (encoded by *mrcB*) across a range of drug and
137 environmental stress conditions. This approach previously identified LpoB, the OM lipoprotein activator
138 of PBP1B (Typas *et al.*, 2010). $\Delta cpoB$ exhibited the second highest correlation with $\Delta mrcB$ (Fig. 1A;
139 correlation coefficient = 0.47, $p < 10^{-18}$), suggesting that CpoB may also be functionally associated with
140 PBP1B. CpoB (YbgF) is encoded by the last gene in the *tol-pal* operon and binds TolA *in vitro* (Krachler
141 *et al.*, 2010), but its deletion does not cause the severe OM integrity defects typically associated with
142 *tol-pal* deletions (Vianney *et al.*, 1996). Thus, CpoB is not critical for Tol-Pal function, and its cellular
143 role has remained enigmatic.

144

145 $\Delta cpoB$ and $\Delta mrcB$ mutants shared increased sensitivities to certain β -lactams (Fig. 1A),
146 particularly cefsulodin, which preferentially inhibits PBP1A. As loss of both PBP1A and PBP1B function
147 is synthetically lethal (Yousif *et al.*, 1985), the enhanced cefsulodin sensitivity of $\Delta cpoB$ likely derives
148 from defects in PBP1B function or regulation unmasked by loss of PBP1A function. Consistent with

149 this idea, overexpression of PBP1B abrogated the cefsulodin sensitivity of $\Delta cpoB$ (Fig. 1B). Additionally,
150 both $\Delta cpoB$ and $\Delta mrcB$ mutants exhibited increased lysis in an envelope stability screen (Paradis-
151 Bleau *et al.*, 2014). Importantly, the lysis phenotype of a $\Delta cpoB \Delta mrcB$ did not exceed that of the
152 $\Delta mrcB$ single mutant (Fig. S1A-B). This epistatic relationship strongly suggests that CpoB acts via
153 PBP1B. Finally, using periplasmic mCherry to fluorescently visualize envelope morphology (Gerding *et*
154 *al.*, 2007) we found that both $\Delta mrcB$ and $\Delta cpoB$ cells exhibited elevated levels of OM defects,
155 particularly OM blebbing (Fig. 1C-D).

156
157 We further tested the proposition that lack of CpoB leads to defective PBP1B function using
158 double mutant analysis. As LpoA is essential for PBP1A function *in vivo*, lack of LpoA is synthetically
159 lethal with lack of PBP1B (Typas *et al.*, 2010, Paradis-Bleau *et al.*, 2010). Consistent with CpoB
160 involvement in PBP1B function, a strain lacking both LpoA and CpoB showed a severe growth defect
161 (Fig. 1F) and exacerbated envelope defects, including extensive cell lysis (Fig. 1C-E and S1A-C). All of
162 these effects were ameliorated by overexpression of PBP1B (Fig. 1C-F). Of note, the envelope defects
163 of $\Delta cpoB \Delta lpoA$ were distinct from those of *tol-pal* mutants (Gerding *et al.*, 2007), with more extensive
164 lysis but less OM blebbing and periplasmic leakage (Fig. 1C-E and S1C). Taken together, these results
165 validate the idea that CpoB contributes to proper PBP1B function *in vivo*.

166

Having established a strong functional relationship between CpoB and PBP1B, we asked whether they interact physically *in vivo*. Indeed, we identified CpoB in a screen for novel PBP1B interaction partners, using *in vivo* photo-cross-linking following incorporation of a non-natural amino acid (pBpa) at specific and exposed sites (Chin and Schultz, 2002). Initially focusing on the PBP1B UB2H domain, we identified two sites (T118 and E123) that cross-linked to a protein of approximately 30 kDa (Fig. 2A-B). These sites reside in a cleft between the UB2H and TPase domains. Testing opposing amino acids in the TPase domain (T751 and T753) yielded cross-link products of the same size (Fig. 2A-B). Mass spectrometric analysis of the cross-link bands identified CpoB as a main constituent of the cross-linking product (Table 1). These results imply that PBP1B and CpoB physically interact *in vivo*.

LpoA has a second function that is redundant with CpoB

$\Delta lpoA$ and $\Delta mrcA$ mutants usually exhibit similar phenotypes, consistent with the known role of LpoA in PBP1A activation (Paradis-Bleau *et al.*, 2010, Typas *et al.*, 2010). We therefore expected that a strain lacking both PBP1A and CpoB ($\Delta mrcA \Delta cpoB$) would exhibit the same aggravated growth and envelope defects as the $\Delta lpoA \Delta cpoB$ strain. However, this was not the case (Fig. S2; Fig S3B-D), suggesting that LpoA not only activates PBP1A, but also has a second function that compensates for loss of CpoB.

186 LpoA has two separable domains, an N-terminal tetratricopeptide repeat (TPR) domain and a C-
187 terminal domain (Fig. S3A; (Jean *et al.*, 2014, Typas *et al.*, 2010)). We found previously that the C-
188 terminal domain is sufficient to bind and activate PBP1A *in vitro* (Typas *et al.*, 2010). We verified that
189 the same is true *in vivo* by showing that cells lacking PBP1B and possessing only C-terminal domain of
190 LpoA were healthy ($\Delta mrcB$ *lpoA*(ΔTPR), Fig. S2B). We then asked whether the N-terminal TPR domain
191 of LpoA, being dispensable for PBP1A activation, might instead mediate the CpoB compensatory
192 function of LpoA. This indeed proved to be the case, as a $\Delta cpoB$ $\Delta mrcA$ *lpoA*(ΔTPR) triple mutant
193 recapitulated the growth and envelope defects of the $\Delta cpoB$ $\Delta lpoA$ mutant (Fig. S3B-D). Note that since
194 these phenotypes are unmasked in the absence of PBP1A function, and LpoA(ΔTPR) can still activate
195 PBP1A, a $\Delta cpoB$ *lpoA*(ΔTPR) double mutation alone does not recapitulate the phenotypes of $\Delta cpoB$
196 $\Delta lpoA$. The fact that the N-terminal TPR domain of LpoA functionally compensates for lack of CpoB
197 thus explains why $\Delta lpoA$ and $\Delta mrcA$ mutants differ in this particular phenotype. We present this finding
198 to make our double mutant results understandable, but do not pursue it further in this work, which
199 focuses on the role of CpoB.

200

201 **CpoB localizes to the septum late in cell division, coincident with the onset of OM constriction**

202 We next investigated whether CpoB, like PBP1B and Tol-Pal (Bertsche *et al.*, 2006, Gerding *et*
203 *al.*, 2007), is recruited to the septum. Using a functional, endogenously expressed CpoB-mCherry
204 fusion protein (Fig. S4A), we observed that CpoB localized at sites of visible envelope constriction in

205 pre-divisional cells (Fig. 3A), and was positioned preferentially at mid-cell with increasing prevalence as
206 the cell cycle progressed (Fig. 3B-C). This pattern of localization was corroborated for the native protein,
207 as visualized by immunolabeling cells with antibody specific to CpoB (Fig. S5). Mid-cell positioning of
208 CpoB-mCherry was coincident with envelope constriction (Fig. 3A-D), suggesting a role during that
209 stage of cell division.

210

211 Tol-Pal localizes at constriction sites during later stages of cell division (Gerding *et al.*, 2007). To
212 better define the timing of CpoB recruitment, we compared the cell cycle dynamics of septal CpoB-
213 mCherry localization with that of other divisome components (Fig. 3B, D). As cell length correlates with
214 cell cycle progression, measuring fluorescence enrichment at mid-cell in cells sorted by length provides
215 a quantitative metric for temporal comparison (den Blaauwen *et al.*, 1999, Aarsman *et al.*, 2005, van
216 der Ploeg *et al.*, 2013). FtsZ initiates cell division and divisome assembly, with PBP3 and FtsN
217 localizing at progressively later stages (van der Ploeg *et al.*, 2013) (Fig. 3B, D; Fig. S6); FtsN is the last
218 essential component recruited in the divisome (Aarsman *et al.*, 2005). CpoB-mCherry, a functional
219 TolA-GFP fusion (Fig. S4B), PBP1B, LpoB, and FtsN localized at approximately the same time (Fig. 3B,
220 D). Thus, CpoB is recruited to the septum during the later stages of cell division, concurrent with Tol-
221 Pal, PBP1B, and the onset of OM constriction.

222

223 We next asked which proteins and cell division events are required for recruitment of CpoB to
224 the septum. CpoB failed to localize in cells with temperature-sensitive (ts) FtsZ, FtsA, FtsW, or PBP3
225 under non-permissive conditions, and in cells depleted for FtsN, indicating that CpoB localization is
226 dependent on divisome assembly (Fig. S7A-F). CpoB also failed to localize following inhibition of PBP3
227 with aztreonam (Fig. S7G), indicating that its localization also requires ongoing septal PG synthesis.
228 However, CpoB localized normally in the absence of PBP1B (Fig. S8A). TolA dependence was more
229 difficult to examine, since delayed OM constriction in the absence of TolA leads to the non-specific
230 accumulation of periplasmic proteins at cell division sites (Gerding *et al.*, 2007). Under growth
231 conditions that minimized this effect, CpoB continued to localize in the absence of TolA (Fig. S8B),
232 suggesting that it can be recruited independently of TolA. Because a strain lacking PBP1B and TolA is
233 only marginally viable (Typas *et al.*, 2010), we cannot distinguish whether CpoB localization is
234 independent of both PBP1B and TolA, or whether each partner alone is sufficient to drive CpoB
235 localization.

236

237 CpoB localization is thus tied to cell division. Further, CpoB interacts and co-localizes with
238 proteins involved in both OM constriction (TolA; (Krachler *et al.*, 2010, Gerding *et al.*, 2007)) and PG
239 septal synthesis (PBP1B; Fig. 2), raising the possibility that CpoB participates in coupling these
240 processes following recruitment to the septum during cell division.

241

242 **CpoB, TolA, PBP1B, and LpoB form a complex**

243 Interactions between TolA and CpoB (Krachler *et al.*, 2010) and between PBP1B and LpoB
244 (Paradis-Bleau *et al.*, 2010, Typas *et al.*, 2010) have been previously reported. We searched for
245 associations between these complexes that might facilitate functional coordination by testing for further
246 direct pairwise interactions between these proteins *in vitro*. As measured by surface plasmon
247 resonance (SPR), CpoB bound to immobilized PBP1B with a dissociation constant (K_D) of 325 ± 43 nM,
248 but not to PBP1A or to a surface without protein (Fig. 4A-B), indicating a direct and specific interaction.
249 PBP1B and TolA also interact directly, as untagged TolA was retained on Ni-NTA beads in the
250 presence but not absence of His6-PBP1B (Fig. 4C). A purified soluble version of TolA lacking its
251 transmembrane anchor (domain I) was not pulled down with His6-PBP1B (Fig. 4C), indicating that
252 domain I of TolA is required for interaction. In contrast, LpoB does not bind either CpoB or TolA directly,
253 as a His-tagged version of LpoB did not retain CpoB or TolA on Ni-NTA beads, while retaining PBP1B
254 as expected (Fig. S9A).

255

256 To contextualize these pairwise interactions, we assessed higher order interactions. As CpoB
257 and TolA each interact with PBP1B, we tested whether they also formed a ternary complex. Indeed,
258 chemically cross-linking a mixture of PBP1B, TolA, and CpoB identified a high-molecular weight
259 species containing all three proteins (Fig. S9B). Using this technique, we did not detect analogous high
260 molecular weight complexes of PBP1A with TolA or CpoB (Fig. S9B), confirming that the CpoB and

261 TolA interactions and complex formation with PBP1B were specific. Since LpoB is required for PBP1B
262 activation *in vivo*, we next tested whether CpoB and TolA interact with PBP1B in complex with LpoB.
263 Indeed, in the presence but not absence of PBP1B, His-LpoB retained CpoB and TolA on Ni-NTA
264 beads after chemical cross-linking, indicating that LpoB-PBP1B-CpoB and LpoB-PBP1B-TolA form
265 ternary complexes (Fig. S9A). Given that all possible ternary complexes containing PBP1B can be
266 formed, we propose that PBP1B, LpoB, CpoB, and TolA can also form a quaternary complex.

267

268 As CpoB can form a complex with both PBP1B-LpoB and TolA, its cellular abundance might
269 influence which interactions occur *in vivo*. Using purified protein as a standard and an antibody specific
270 to CpoB, we determined a CpoB cellular copy number of 4550 ± 540 ($n = 5$) in growing cells (Fig. S10).
271 This is similar to an estimated protein synthesis rate for CpoB of ~5200 molecules per generation,
272 determined via ribosome profiling (Li *et al.*, 2014). Thus, the abundance of CpoB significantly exceeds
273 the ~520 molecules of PBP1B and ~480 molecules of TolA synthesized per generation (Li *et al.*, 2014).
274 CpoB forms trimers, which disassociate to the monomeric form when bound to TolA (Krachler *et al.*,
275 2010); it is unclear in what form(s) CpoB binds to PBP1B. Nevertheless, even in its trimeric form
276 (~1500 trimers), CpoB is in excess to both PBP1B and TolA, and is therefore likely able to interact
277 constitutively with both partners.

278

279 Taken together, these data suggests that CpoB, PBP1B-LpoB, and Tol-Pal associate to form a
280 higher-order complex, spatially linking PG synthesis and OM constriction during cell division.

281

282 **CpoB and TolA modulate PBP1B-mediated PG synthesis**

283 We tested the effects of TolA and CpoB on PBP1B GTase and TPase activities *in vitro*. As
284 measured by consumption of fluorescently labeled lipid II substrate (Fig. 5A and S11A), TolA increased
285 the GTase rate of PBP1B 1.9 ± 0.5 -fold, indicating that TolA is a novel regulator of PBP1B. Although
286 weaker than the 8-fold stimulation by LpoB (Fig. 5A; (Egan *et al.*, 2014)), TolA and LpoB stimulation
287 were additive, together yielding an 11.3 ± 0.5 -fold increase in GTase activity. These results indicate that
288 LpoB and TolA stimulate PBP1B GTase by compatible mechanisms. In contrast, CpoB had no effect on
289 the GTase activity of PBP1B, alone or in combination with LpoB and/or TolA (Fig. 5A). Neither CpoB
290 nor TolA affected basal PBP1B TPase activity (Fig. 5B, orange), as quantified by % of peptides with
291 cross-links in PG produced with radiolabelled lipid II as substrate. Note that, unlike for GTase activity, a
292 continuous TPase assay is currently not available, and therefore we cannot rule out that one of the two
293 proteins affects the TPase rate of PBP1B; this would in fact be expected for TolA as a consequence of
294 the GTase activation (see below).

295

296 The GTase and TPase activities of PBP1B are coupled, as is generally true for bifunctional
297 synthases (Bertsche *et al.*, 2005, Born *et al.*, 2006, Lupoli *et al.*, 2014). LpoB activates both the PBP1B

298 GTase domain, increasing reaction rate, and the TPase domain, thereby producing hyper-cross-linked
299 PG (Fig. 5B, blue) (Typas *et al.*, 2010, Egan *et al.*, 2014). Interestingly, although CpoB did not affect the
300 cross-linking activity of PBP1B on its own, it partially prevented the formation of hyper-cross-linked PG
301 in the presence of LpoB (Fig. 5B, blue). As CpoB affected neither LpoB binding to PBP1B (Fig. S9A)
302 nor GTase stimulation of PBP1B (Fig. 5A), CpoB must directly interfere with PBP1B TPase activation
303 by LpoB. Strikingly, TolA alleviated this effect of CpoB, restoring the synthesis of highly cross-linked PG
304 in the presence of LpoB (Fig. 5B, cyan). The effects of CpoB and TolA on TPase activity were further
305 enhanced at a moderately increased salt concentration (215 mM NaCl): under this condition, CpoB
306 completely prevented PBP1B from synthesizing hyper-cross-linked PG, and TolA again completely
307 alleviated this effect (Fig. 5B, right graph). This suggests that their regulation of PBP1B may be
308 responsive to stress or other perturbations. In summary, interaction of the PBP1B-LpoB synthase
309 complex with TolA further stimulates the PBP1B GTase activity, and interactions with CpoB and TolA
310 modulate PBP1B TPase activity via reciprocal effects.

311

312 **Regulation of PBP1B by CpoB and TolA responds to Tol-Pal energy state *in vivo*.**

313 To establish *in vivo* relevance and to understand how complex formation and PBP1B activity are
314 regulated *in vivo*, we systematically characterized interactions between CpoB, TolA, PBP1B, and LpoB
315 via DTSSP cross-linking and co-immunoprecipitation (Fig. 6A-C). In addition to the previously reported
316 PBP1B-LpoB pair (Typas *et al.*, 2010), we observed specific pairwise interactions between CpoB, TolA,

317 and PBP1B, validating that these interactions also occur *in vivo*. Interestingly, CpoB exhibited minimal
318 or no cross-linking with LpoB in the presence of TolA, but a dramatic increase in cross-linking in its
319 absence (Fig. 6A). Thus, TolA both prevents CpoB from associating with LpoB (Fig. 6A) and from
320 interfering with PBP1B TPase stimulation by LpoB (Fig. 5B), suggesting that these effects are linked.
321 Since an interaction between CpoB and LpoB was not detected *in vitro* (Fig. S7A), their association *in*
322 *vivo* likely occurs in the context of the CpoB-PBP1B-LpoB ternary complex (Fig. 7A). This possibility
323 could not be tested directly because a strain lacking both PBP1B and TolA is only marginally viable
324 (Typas *et al.*, 2010). TolA did not prevent PBP1B from interacting with CpoB (Fig. 6A); thus, interaction
325 with TolA may instead alter the conformation of CpoB in a manner that both prevents it from interacting
326 with LpoB (Fig. 6A) and, concurrently, from modulating PBP1B TPase activation by LpoB (Fig. 5B).

327

328 PBP1B-CpoB-TolA complex formation was highly responsive to Tol-Pal status. In the absence
329 of TolQ, abrogating formation of the TolQR-TolA complex, PBP1B-TolA and PBP1B-CpoB interactions
330 were both substantially diminished. In contrast, CpoB-LpoB interaction and PBP1B-LpoB complex
331 formation increased significantly (Fig. 6A). Together, these data suggested that CpoB regulates
332 PBP1B-LpoB in response to the Tol-Pal assembly state, energy state, or both. To distinguish between
333 these possibilities, we compared the effects of a *tolR* deletion, which prevents TolQR-TolA complex
334 assembly, to those of a *tolR(D23R)* point mutation that allows complex assembly but prevents TolQR
335 from utilizing PMF and thus energizing TolA (Cascales *et al.*, 2001). In the *tolR(D23R)* mutant,

336 interaction between TolA and PBP1B was maintained (Fig. 6B), suggesting that physical association
337 between the PBP1B-LpoB and Tol-Pal complexes depends on assembly of the TolQR-TolA complex *in*
338 *vivo* but not on its energy state. In contrast, interaction between CpoB and LpoB was highly elevated
339 (Fig. 6B). This strongly suggests that TolA must be energized to prevent CpoB both from interacting
340 with LpoB and, in conjunction, from inhibiting PBP1B TPase stimulation by LpoB. This implies that
341 cycles of TolQR PMF utilization that energize TolA can in turn modulate PBP1B TPase activity, allowing
342 dynamic regulation of PBP1B activity in response to Tol-Pal energy state.

343

344 Taken together, interactions between PBP1B-LpoB, Tol-Pal, and CpoB promote physical and
345 spatial coordination of PBP1B-LpoB and Tol-Pal, and provide a mechanism for direct regulation of
346 septal PG synthesis in response to Tol-Pal function.

347 **DISCUSSION**

348

349 Despite major progress understanding bacterial cell division, it has remained unknown how
350 Gram-negative bacteria coordinate OM invagination with IM invagination and septal synthesis. In this
351 work, we present a mechanism for coordinating PG synthesis and OM constriction, featuring CpoB,
352 previously of unknown function, as its centerpiece. We demonstrate that CpoB bridges these processes,
353 promoting physical and functional coordination of the PBP1B-LpoB and Tol-Pal machineries, which
354 operate respectively at the closely-spaced front and back ends of the invaginating envelope. We found
355 that both CpoB and TolA interact directly with PBP1B, and our *in vitro* data supports formation of a
356 higher order complex (Fig. 7A). As depicted in our summary model, interactions between PBP1B, LpoB,
357 CpoB, and TolA allow for dynamic regulation of PBP1B activity, and thus functional coordination of the
358 PBP1B and Tol-Pal machineries (Fig. 7B). Below, we first discuss how interaction between these
359 machineries tunes PG synthesis, and then indicate the physiological importance of this process. We
360 end with an evolutionary perspective on these findings.

361

362 **How CpoB tunes PBP1B-LpoB function to the Tol-Pal cycle**

363 In the absence of input from CpoB, LpoB binding to PBP1B stimulates both its GTase and
364 TPase activities. TPase activation results in hyper-cross-linked PG, containing ~70% cross-linked
365 peptides *in vitro* (Fig. 7B top, left). CpoB binding interferes only with TPase stimulation (Fig. 7B, top

366 right), so that ~60% of the peptides are cross-linked. Importantly, this level of cross-linking is similar to
367 that observed in mini-cells, which are formed by abnormal polar divisions *in vivo* and have an
368 exclusively polar PG (Obermann and Holtje, 1994). Therefore, CpoB reduces cross-linkage to a more
369 physiological level. This may be the default cellular state as CpoB is present in ~10-fold excess over its
370 PBP1B and TolA binding partners (Fig. S10 and (Li *et al.*, 2014)). CpoB is the first example of an
371 endogenous regulator that can control the TPase activity of a bifunctional PG synthase, independently
372 of its GTase activity. It thus mimics the activity of penicillin G, which blocks PBP1B TPase activity
373 without interfering with GTase stimulation by LpoB (Lupoli *et al.*, 2014).

374

375 TolA further modulates PBP1B function by reversing CpoB inhibition, in a manner that is
376 dependent on Tol-Pal status (Fig. 7B, bottom panels). Fuelled by PMF-derived energy, Tol-Pal cycles
377 between at least two alternative states; we propose that each state has distinct functional
378 consequences for PG synthesis. During the non-energized phase of Tol-Pal function, CpoB inhibits
379 LpoB-mediated PBP1B TPase hyper-activation (Fig. 7B, bottom right). During the energized phase,
380 however, TolA adopts a new conformation that allows it to alleviate CpoB inhibition, thereby restoring
381 maximal TPase stimulation by LpoB (Fig. 7B, bottom left). Thus, CpoB provides the means to
382 selectively regulate PBP1B catalytic activities, and TolA modulates this effect, linking cycles of PBP1B
383 activity state and the resulting PG cross-linking with the cycles of Tol-Pal energy state and OM
384 invagination.

385

386 TolA also directly stimulates PBP1B GTase activity, independent of and additively with LpoB.

387 We do not yet know whether this stimulation occurs during one or both phases of Tol-Pal function.

388 Importantly, recruitment and assembly of the TolQRA IM sub-complex is required for regulation of

389 PBP1B by TolA *in vivo*: in the absence of TolQ or TolR, interaction between TolA and PBP1B is

390 significantly decreased, whereas interaction between PBP1B and LpoB is enhanced. TolQ and TolA

391 localize to the septum independent of each other (Gerding *et al.*, 2007), and their recruitment may

392 incorporate different regulatory cues.

393

394 **Why is PBP1B tuning necessary for coordinating septal PG synthesis and OM constriction?**

395 We propose that selectively tuning the GTase and TPase activities of PBP1B offers functional

396 flexibility that is particularly important during constrictive PG synthesis. PBP1B-LpoB has the capacity

397 to produce highly cross-linked PG, which may be required at certain stages of new pole synthesis, but

398 the TPase activity of PBP1B is normally down-regulated by CpoB. Up-regulation is allowed only at

399 specific step(s) of the Tol-Pal cycle. Thus, for PBP1B-LpoB at the septal leading edge, increased cross-

400 linking (TPase) activity is permitted only when the OM is brought into close proximity via cycles of Tol-

401 Pal function and energy utilization, allowing energized TolA to counteract CpoB. The IM-bound septal

402 leading edge can thereby sense directly the status of the ingrowing end of the constricting envelope

403 (OM), and the cycles of the two machineries are synchronized to ensure a constant distance between

404 the OM and IM. Restricting TPase activity based on Tol-Pal progress may also promote better
405 coordination of septal PG synthesis and septal cleavage by OM-controlled amidases (Uehara *et al.*,
406 2010, Yang *et al.*, 2011).

407

408 By making PBP1B activity responsive to the presence, assembly and energy state of Tol-Pal,
409 CpoB facilitates feedback regulation of PG synthesis based on the status of OM invagination. The
410 importance of such coordination can be seen when it is broken, as demonstrated by the phenotypes of
411 a strain lacking CpoB. Antibiotic sensitivities, envelope defects, and genetic interactions paralleling
412 those of a strain lacking PBP1B suggested that CpoB contributes to proper PBP1B function *in vivo*, an
413 interpretation bolstered by the facts that PBP1B overexpression alleviated these $\Delta cpoB$ phenotypes
414 and a strain lacking both proteins phenocopied a PBP1B mutant. This apparent loss of PBP1B function
415 may result from loss of proper coordination with Tol-Pal that is required for efficient and productive
416 utilization of PBP1B activity during septation. In addition, loss of TPase modulation may itself be
417 deleterious, as uncontrolled PG synthase activity can be as detrimental to the cell as no activity (Cho *et*
418 *al.*, 2014). Synthetic and hydrolytic enzymatic reactions have to be carefully balanced for seamless PG
419 growth, a principle exploited by β -lactam antibiotics, which lyse cells predominantly via uncontrolled PG
420 hydrolase activity (Kohlrausch and Holtje, 1991). In this scenario, overexpression of PBP1B may
421 alleviate $\Delta cpoB$ phenotypes by ensuring that there is enough unbound (hypoactive) PBP1B in the cell
422 to counter-balance hyperactive PBP1B-LpoB in septal PG synthesis.

423

424 Coordination of the PBP1B and Tol-Pal machines by CpoB may also be important for proper
425 Tol-Pal function. Defects in OM integrity in the absence of PBP1B or CpoB are consistent with such a
426 role. The molecular mechanism of Tol-Pal-mediated OM constriction remains poorly defined (Egan and
427 Vollmer, 2013, Gerding *et al.*, 2007), and the system is currently not amenable to *in vitro* dissection. It is
428 thus more difficult to determine specific regulatory effects of CpoB and PBP1B on Tol-Pal activity.
429 However, coordination likely promotes synchronous OM constriction during cell division, and reciprocal
430 regulation of Tol-Pal activity would allow bidirectional coordination of function. Since PBP1B-LpoB can
431 partially compensate for loss of Tol-Pal (Typas *et al.*, 2010), it is possible that the two complexes
432 mediate OM constriction cooperatively.

433

434 **Specificity and modularity in PG synthase evolution**

435 PBP1B and PBP1A retain some core functional redundancy, which allows cell survival when
436 only one is present (Yousif *et al.*, 1985). This partial redundancy adds robustness to cell wall
437 biosynthesis. However, PBP1B and PBP1A also have distinct roles.. PBP1B is adapted to play a key
438 role in cell division in *E. coli*, as illustrated by phenotypic, localization, and physical interaction data
439 (Bertsche *et al.*, 2006, Muller *et al.*, 2007, Typas *et al.*, 2010), and by the fact that cells without PBP1B
440 lyse from the mid-cell at a higher frequency (Garcia del Portillo and de Pedro, 1990). Here we provide
441 additional evidence for the specialized role of PBP1B-LpoB complex in cell division, as it interacts and

442 physically coordinates its function with Tol-Pal (Gerding *et al.*, 2007). Physical and regulatory
443 interactions thus link PBP1B to septal PG synthesis (PBP3, FtsN, FtsW (Bertsche *et al.*, 2006, Muller *et*
444 *al.*, 2007, Fraipont *et al.*, 2011)), PG hydrolysis (MltA (Vollmer *et al.*, 1999)), and now OM constriction
445 (Tol-Pal and CpoB), integrating division processes that span the envelope. Multiple divisome-
446 associated regulators (FtsN, LpoB, CpoB, TolA) either stimulate or inhibit PBP1B activity. Regulation by
447 other factors may be synergistic or antagonistic with regulation by CpoB and Tol-Pal, or alternatively
448 may be employed at different stages of septation, helping PBP1B to further address unique
449 requirements of constrictive PG synthesis.

450

451 PBP1B and other PG-related enzymes (e.g., amidases (Uehara *et al.*, 2009)) are often
452 characterized by modular architectures, combining broadly conserved catalytic domains with
453 evolutionarily confined non-catalytic domains. We have proposed that these non-catalytic domains
454 provide specificity and diversification to the enzymes (Typas *et al.*, 2012). In the case of PBP1B, the
455 non-catalytic UB2H domain shares an extensive binding interface with LpoB (Egan *et al.*, 2014), and as
456 we show here, is also involved in binding CpoB. Interestingly, LpoB and CpoB approach UB2H from
457 different sides (Fig. 7A), consistent with their independent binding to PBP1B. CpoB and LpoB come
458 close in this conformation, and this proximity could facilitate the LpoB-CpoB interaction, which is
459 stabilized in the non-energized state of the Tol-Pal system. As the UB2H domain and LpoB are present
460 only in enterobacteria and Vibrionaceae (Typas *et al.*, 2010, Dörr *et al.*, 2014), it remains to be

determined whether and how the more conserved Tol-Pal system is integrated with septal PG synthesis in other bacteria. Interestingly, CpoB is not conserved in all bacteria with a Tol-Pal system, or even in some that contain LpoB (e.g., Pasteurellaceae).

464

We postulate that other niche-specific factors will tightly coordinate PG septal synthesis and constriction of the different envelope layers in microbes that lack CpoB and/or LpoB. In this regard, our finding that LpoA has an additional function beyond activating PBP1A, one that is redundant with (or otherwise exacerbates the need for) CpoB, is particularly interesting. It extends for the first time the principle of modularity to PG enzyme regulators, as LpoA has two physically separated domains: one for binding and activating PBP1A (C-terminal domain) and one for its CpoB-related function (N-terminal TPR domain). Moreover, as both CpoB and LpoA possess TPR domains, which are generally involved in protein-protein interactions, this raises the question of whether both their TPR domains are involved in additional binding and/or regulation with other PG-related enzymes. A straightforward scenario would be that LpoA can directly link to the Tol-Pal system. In contrast to CpoB, we could not detect a direct interaction between LpoA and soluble TolA *in vitro*. However, the LpoA connection to TolA may be more complex (e.g., dependent on conformational state of TolA), or LpoA may achieve a CpoB-like function via connections to other Tol-Pal components (e.g., TolB or Pal). Such a connection would be consistent with the ability of PBP1A to partially substitute for PBP1B, and with the general role of Tol-Pal in envelope integrity. As all these components (PBP1B/A, LpoB/A, CpoB, and Tol-Pal) localize

independently to division sites, multiple redundant or alternative paths may exist for coordinating PG synthesis and OM constriction, increasing the robustness of the process to function under different conditions and across different organisms.

Conclusion

Physical and functional coordination of PBP1B with Tol-Pal, facilitated by CpoB, reveals an important additional layer in the regulatory circuitry that controls PBP1B function, and paints an increasingly intricate picture of PBP1B as a regulatory scaffold that is uniquely adapted for the coordination of the cell division process in *E. coli*. This is the first mechanistic view of how different envelope layers talk to each other as they grow and constrict during cell division in Gram-negative bacteria. Importantly, the process retains a high degree of modularity, which would allow for individual components to be replaced across evolution, and presumably to some degree in *E. coli* itself. Continued dissection of the dynamic multi-enzyme, membrane-spanning machines that mediate coordinated cell division processes, including investigation of which interactions occur simultaneously, when and where in the cell they occur, and what additional regulatory relationships they confer, will provide greater understanding of the molecular mechanisms that govern interconnected divisome functions and their synchronization. Looking across different organisms will also provide a better overview of which interconnections are broadly required and by what different means they can be achieved. Considering the many facets of cell envelope composition (Radolf *et al.*, 2012) and cell

499 division (Leisch *et al.*, 2012), these questions are bound to have different answers in different bacteria.
500 Nevertheless, the geometric and topological changes inherent during cell division likely generally
501 necessitate a high degree of feedback between the different envelope layers through physical
502 connections that modulate biochemical activities (Weiss, 2015).

503 MATERIALS AND METHODS

504

505 Chemicals and proteins

506 [¹⁴C]GlcNAc-labelled lipid II and dansylated lipid II were prepared as published (Bertsche *et al.*, 2005,
507 Breukink *et al.*, 2003). The following proteins were prepared as previously described: PBP1B (Bertsche
508 *et al.*, 2006), His-LpoB(sol) and LpoB(sol) (Egan *et al.*, 2014). Antisera against PBP1B, LpoB, CpoB,
509 TolA and TolB (rabbit) were obtained from Eurogentec and purified over an antigen column as
510 described (Bertsche *et al.*, 2006). Cellosyl was provided by Hoechst AG, Frankfurt, Germany. VIM-4
511 was a kind gift from Adeline Derouaux.

512 Protein overproduction and purification

513 BL21(DE3) strains harbouring plasmids pET28-His6-CpoB (for the purification of CpoB; signal
514 sequence replaced by an oligohistidine tag), pET28-TolA-His6 (for the purification of full length TolA
515 with a C-terminal oligohistidine tag), pET28-His6-TolA (for the purification of full length TolA with a
516 cleavable N-terminal oligohistidine tag) or pET28-His6-TolA(sol) (for purification of TolA(72-421)) were
517 grown in 3 L of LB medium with appropriate supplements at 30°C to an OD₅₇₈ of 0.5 - 0.6. Recombinant
518 genes were overexpressed by adding 1 mM IPTG to the cell culture followed by a further incubation for
519 3 h at 30°C. Cells were harvested by centrifugation (10,000 × g, 15 min, 4°C) and the pellet was
520 resuspended in buffer I (25 mM Tris/HCl, 10 mM MgCl₂, 500 mM NaCl, 20 mM imidazole, 10% glycerol,
521 pH 7.5). A small amount of DNase, protease inhibitor cocktail (Sigma, 1/1000 dilution) and 100 μM

phenylmethylsulfonylfluoride (PMSF) was added before cells were disrupted by sonication (Branson digital). The lysate was centrifuged ($130,000 \times g$, 1 h, 4°C). At this point, purification procedures of full length TolA constructs and of CpoB and TolA(sol) differ.

For CpoB and TolA(sol) the supernatant was applied to a 5 mL HisTrap HP column (GE healthcare), attached to an ÄKTA Prime⁺ (GE Healthcare), at 1 ml/min. The column was washed with 4 volumes buffer I before step-wise elution of bound proteins with buffer II (25 mM Tris/HCl, 10 mM MgCl₂, 500 mM NaCl, 400 mM imidazole, 10% glycerol, pH 7.5). To remove the oligohistidine tag from His-CpoB and His-TolA(sol), 50 U/mL of restriction grade thrombin (Novagen) was added and the protein which was then dialyzed against 2 L of 25 mM Tris/HCl, 10 mM MgCl₂, 500 mM NaCl, 10% glycerol, pH 7.5 for 18 h at 4°C. Proteins samples were then concentrated to 4 - 5 mL using a VivaSpin-6 column (MW cut-off 6,000 Da) and applied to a Superdex200 HiLoad 16/600 column at 0.8 mL/min for size exclusion chromatography in 25 mM Tris/HCl, 1 M NaCl, 10% glycerol, pH 7.5. Finally, proteins were dialyzed against storage buffer (25 mM Tris/HCl, 500 mM NaCl, 10% glycerol, pH 7.5).

For full length TolA or TolA-His, the membrane pellet resulting from the above ultracentrifugation was resuspended in extraction buffer (25 mM Tris/HCl, 10 mM MgCl₂, 1 M NaCl, 2% Triton X-100, 10% glycerol, pH 7.5) and incubated overnight with mixing at 4°C. Samples were centrifuged ($130,000 \times g$, 1 h, 4°C) and the supernatant applied to a 5 ml HisTrap HP column (GE healthcare) attached to an ÄKTA Prime⁺ (GE Healthcare), at 1 mL/min. The column was washed with 4 volumes extraction buffer, followed by 4 volumes of wash buffer I (25 mM Tris/HCl, 10 mM MgCl₂, 20

541 mM imidazole, 2% Triton X-100, 10% glycerol, pH 7.5), followed by a final wash with 4 volumes of wash
542 buffer II (as wash buffer I, with 40 mM imidazole and 0.2% Triton X-100). Bound protein was eluted
543 step-wise with elution buffer (25 mM Tris/HCl, 10 mM MgCl₂, 500 mM NaCl, 400 mM imidazole, 0.2%
544 Triton X-100, 10% glycerol, pH 7.5). At this point, TolA-His was dialysed into storage buffer (25 mM
545 Tris/HCl, 500 mM NaCl, 0.2% Triton X-100, 10% glycerol, pH 7.5). To remove the oligohistidine tag
546 from His-TolA, 50 U/ml of restriction grade thrombin (Novagen) was added to the protein which was
547 then dialyzed against 2 L of 25 mM HEPES/NaOH, 10 mM MgCl₂, 50 mM NaCl, 10% glycerol, pH 6.0
548 for 24 h at 4°C. Sample was then applied to a 5 ml HiTrap HP SP column attached to an ÄKTA Prime+
549 (GE Healthcare) for ion exchange chromatography, at a flow rate of 0.5 mL/min in buffer A (25 mM
550 HEPES/NaOH, 10 mM MgCl₂, 50 mM NaCl, 0.2% Triton X-100, 10% glycerol, pH 6.0). The column was
551 washed with 6 volumes buffer A before stepwise elution of bound TolA with buffer B (as A, with 500 mM
552 NaCl). TolA sample was then dialysed into storage buffer (25 mM HEPES/NaOH, 10 mM MgCl₂, 100
553 mM NaCl, 0.2% Triton X-100, 10% glycerol, pH 7.5). Recombinant PBP1B (pDML924; the functional,
554 short PBP1B version, starting from amino acid 46) was purified as described previously (Bertsche *et*
555 *al.*, 2005). Versions of proteins retaining their His-tags were purified as above, omitting the addition of
556 thrombin.

557

558 **Bacterial strains, plasmids and growth conditions**

Bacterial strains and plasmids used in this work are listed in Supplementary File 1A. Primers used in this work are listed in Supplementary File 1B.

Growth conditions

For *in vivo* assays, cells were grown aerobically at 30°C or 37°C in Lennox Luria-Bertani (LB) medium (10 g/L tryptone, 5 g/L yeast extract, 5 g/L NaCl) (Fisher) unless otherwise indicated. Where appropriate, antibiotics or inducers were added: ampicillin (100 µg/ml), chloramphenicol (10-34 µg/ml), kanamycin (30 µg/ml), arabinose (0.2% - 1%, w/v), IPTG (1 mM). For protein production, cells were grown aerobically at 30°C or 37°C in Miller LB medium (10 g/L tryptone, 5 g/L yeast extract, 10 g/L NaCl).

Construction of *E. coli* strains

To generate and combine *E. coli* gene deletions, *kan*-marked alleles from the Keio *E. coli* single-gene knockout library (Baba *et al.*, 2006) were transferred into relevant background strains using P1 phage transduction (Thomason *et al.*, 2007). The Keio pKD13-derived *kan* cassette is flanked by FRT sites, allowing removal of the *kan* marker via expression of FLP recombinase to generate unmarked (kanamycin-sensitive) deletions with a FRT-site scar sequence (Baba *et al.*, 2006, Datsenko and Wanner, 2000).

Other chromosomal mutations and gene fusions (*lpoA*(Δ 58-252), *tolQ*(D23R), *cpoB-mCherry*, and *gfpmut2-tolA*) were generated via lambda Red recombinase-mediated oligonucleotide and/or PCR recombineering (Thomason *et al.*, 2014) using recombineering plasmid pSIM19 (Datta *et al.*, 2006).

Desired mutations were confirmed by PCR and sequencing. To generate the *lpoA*(Δ 58-252) strain, a *sacB-kan* cassette from plB279 (Blomfield *et al.*, 1991) was amplified using primers ANG014 x ANG015 and inserted into *lpoA* to generate precursor strain CAG70134 (BW25113 *lpoA*(Δ 1-255::(*sacB-kan*)). A PCR product containing the *lpoA*(Δ 58-252) allele was then generated via overlap extension ('stitching') PCR (Heckman and Pease, 2007), using PCR primers ANG235 x ANG239 and ANG241 x ANG242 with *E. coli* genomic DNA as template for the first round of PCR and ANG235 x ANG242 with first-round-PCR-products as template for the second round of PCR. The PCR product was then used to replace the *sacB-kan* cassette via counterselection on no-salt LB plates (10 g/L tryptone 5 g/L yeast extract 18 g/L agar) containing 7% (w/v) sucrose. To generate the *tolQ*(D23R) strain, a *sacB-cat* cassette from plasmid pDS132 (Philippe *et al.*, 2004) was amplified using primers ANG478 x ANG479 and inserted into *tolQ* to generate strain CAG70764 (BW25113 *tolQ*(D23::(*sacB-cat*)). The *tolQ*(D23R) mutation was then introduced by using oligonucleotide ANG484 to replace the *sacB-cat* cassette via sucrose counterselection. To generate the *cpoB-mCherry* strain, *sacB-cat* was inserted after *cpoB* using primers ANG143 x ANG144 and replaced with a GSGSGSGS linker followed by *mCherry* using primers ANG177 x ANG178 with pMG36 (encodes *pal-mCherry*) (Gerding *et al.*, 2007) as template. To generate the *gfpmut2-tolA* strain, *sacB-cat* was inserted before *tolA* using primers ANG263 x ANG264 and replaced with *gfpmut2* followed by an *ATGTRT* linker using primers ANG347 x ANG349 with pBAD24-*gfp* (Nilsen *et al.*, 2004) (encodes *gfpmut2*) as template.

596 To transfer chromosomal mutations and gene fusions to other strain backgrounds, the *sacB-cat*
597 or *sacB-kan* cassette was first transferred to the intended recipient strain by P1 phage transduction
598 (Thomason *et al.*, 2007). The unmarked mutant allele was then transferred into the *sacB-cat* or *sacB-*
599 *kan*-bearing recipient strain by P1 phage transduction with selection on no-salt LB plates containing 7%
600 (w/v) sucrose and 10 mM potassium citrate. (Potassium citrate is substituted for sodium citrate because
601 the addition of sodium prevents *sacB*-mediated sucrose sensitivity.)

602 ***Construction of plasmids***

603 pBAD33-PBP1B was constructed by cloning *mrcB* (encodes PBP1B) along with 20 bp of upstream
604 sequence so as to include the native ribosome binding site (RBS) (PCR primers: ANG093 x ANG094)
605 into the *SacI/XbaI* restriction sites of pBAD33 (Guzman *et al.*, 1995). Similarly, pTolA (pBAD33-TolA)
606 was constructed by cloning *tolA* with 20 bp upstream sequence into *SacI/XbaI* pBAD33 (PCR primers:
607 ANG147 x ANG148). For pET28-His6-CpoB, *cpoB* was cloned into *NdeI/SacI* pET28a (Novagen) (PCR
608 primers: ANG182 x ANG184). For pET28-His6-TolA, *tolA* was cloned into *NdeI/SacI* pET28a, replacing
609 the native GTG *tolA* start codon with the *NdeI* site ATG. For pET28-His6-TolA(sol), *tolA*(74-421) was
610 cloned into *NdeI/SacI* pET28a. For pET28-TolA-His6, *tolA* (without stop codon) was cloned into
611 *NcoI/XhoI*. The forward primer used to amplify *tolA* contained a *BsaI* restriction site, GGTCTCTCATG,
612 to allow cloning into the pET28 *NcoI* site while preserving the native *tolA* sequence after the start codon.

613 Amber (TAG) mutations were introduced in pDML924 using the QuickChange PCR site-directed
614 mutagenesis kit and protocol (Stratagene). PCR reactions were treated with DpnI (Fermentas) to

615 remove parent plasmid and then transformed into *E. coli* DH5 α . Candidate plasmid derivatives
616 containing amber mutations were purified from isolated transformants and confirmed by sequencing.

617

618 **Growth fitness assays** (related to Figs. 1 and S2-S4)

619 *E. coli* gene deletion alleles were derived from the Keio collection (Baba *et al.*, 2006). Strains for
620 overexpressing PBP1B carried arabinose-inducible plasmid pBAD33-PBP1B. *E. coli* wild type and
621 mutant strains were arrayed and grown in a 1536-colony format ($n \geq 96$ for each strain) on LB Lennox
622 plates (20 g/L agar) at 37°C, then replica-pinned robotically (Singer Rotor HDA) to LB Lennox and/or
623 indicated condition plates. Assay plates were incubated for 8-14 h at 37°C and then imaged. Colony
624 sizes were determined using in-house software.

625

626 **Analysis of periplasmic leakage and OM blebbing** (related to Figs. 1 and S3)

627 **Imaging**

628 For DIC and fluorescence imaging for example images (Fig. 1C), cells were imaged at the Nikon
629 Imaging Center (NIC) at UCSF on a Ti-E Microscope with a Plan Apo VC 100x/1.4 Oil (DIC N2 / 100X I)
630 65.4 nm/pixel objective. Images were collected using a Nikon Coolsnap HQ2 camera and NIS-
631 Elements v4.2 software (Nikon Instruments Inc., Melville, NY, USA). For phase-contrast and
632 fluorescence imaging for quantitation (Fig. 1D-E and S3B-C), cells were imaged on a Nikon Eclipse TE
633 inverted fluorescence microscope with a 100X (NA 1.40) oil-immersion objective. Images were

collected using an Andor DC152Q sCMOS camera (Andor Technology, South Windsor, CT, USA) and MicroManager v1.3 software (Edelstein *et al.*, 2010).

Quantitation of periplasmic leakage and OM blebbing

Strains were grown in LB Lennox broth with 1 mM ITPG to induce periplasmic mCherry expression. 1% arabinose and 10 µg/ml chloramphenicol were added for plasmid-bearing strains. Overnight cultures were diluted 1:200 and then grown in a 96-well microplate (Model #780271, Greiner Bio-One) for 2 h before imaging. Phase-contrast images were segmented using a custom MATLAB software package (Ursell *et al.*, 2014). To measure fluorescence profiles along cell outlines, fluorescence intensity was measured along segmented cell contours with a spacing of 1 pixel (0.064 µm). Cells were defined as exhibiting periplasmic leakage if their median contour fluorescence fell below a threshold defined as the 98th percentile of $\Delta toIA$ cell contour fluorescence. To identify blebs, we first located all fluorescent puncta with average brightness above the 99.7th percentile of WT cell brightness, and with an area smaller than 4 µm². Blebs were then defined as isolated bright puncta within 0.3 µm of a segmented cell.

In vivo pBpa cross-linking experiments (related to Fig. 2)

Amber mutations were introduced at indicated sites via site-directed mutagenesis of plasmid pDML924, which encodes His6-tagged PBP1B (Terrak *et al.*, 1999). *E. coli* BL21(DE3) cells were co-transformed with pSup-BpaRS-6TRN (Ryu and Schultz, 2006) and either pDML924 or amber mutant derivatives.

Cells were grown to an OD₆₀₀ of 0.5-0.6; protein production was then induced with 10 µM IPTG and 1 mM freshly-prepared *p*-benzoyl-L-phenylalanine (Bachem) dissolved in 1 M NaOH was added. After 2 h of protein production, cells were harvested by centrifugation, washed with PBS and resuspended in 3 ml PBS, then transferred to a petri dish and exposed to UV light (365 nm) for 1.5 min (photoMax Housing 200W, Oriel Instruments, model 60100, 30 cm distance to sample). Cells were cooled on ice during UV illumination. Cell samples were separated by SDS-PAGE (8%), transferred to a nitrocellulose membrane (BioRad), and analyzed by western blot using monoclonal anti-polyhistidine peroxidase-conjugated antibody (1:4000 dilution, Sigma-Aldrich).

661

662 **Mass spectrometry and related data analysis**

Excised protein bands were reduced with DTT, alkylated with iodoacetamide and in-gel digested with trypsin (Shevchenko *et al.*, 2006). Nanoflow liquid chromatography coupled to mass spectrometry was performed on an Agilent 1200 nanoflow system (Agilent technologies, Amstelveen, The Netherlands) connected to a MS LTQ-Orbitrap XL (Thermo Scientific, Bremen, Germany). The samples were trapped on a 20 mm ReproSil-Pur C18-AQ (Dr. Maisch GmbH, Ammerbuch, Germany) trapping column (packed in-house, i.d., 100 µm; resin, 5 µm) with a flow-rate of 5 µl min⁻¹. Sequential elution of peptides was accomplished using an analytical column (Dr. Maisch GmbH, Germany; packed in-house, i.d., 50 µm; resin, 3 µm) with a 35 min gradient of 10–38% buffer B (buffer A, 0.1 M acetic acid; buffer B, 0.1 M acetic acid, 80% (v/v) acetonitrile) followed by 38–100% B in 3 min, 100% B for 2 min. The flow

rate was passively split from 0.45 mL/min to 100 nL/min (Nesvizhskii *et al.*, 2003). Nanospray was achieved using a distally coated fused silica emitter (made in-house, o.d. 375 µm; i.d. 20 µm) biased to 1.7 kV. Mass spectrometer was operated in the data dependent mode to automatically switch between MS and MS/MS. The high resolution survey full scan was acquired in the orbitrap from m/z 350 to m/z 1500 with a resolution of 30,000 (FHMW). The most intense ions at a threshold of above 500 were fragmented in the linear ion trap using collision-induced dissociation at a target value of 10,000.

Peak lists were generated from the raw data files using the Proteome Discoverer software package version 1.3.339 (Thermo Scientific, Bremen, Germany). Peptide identification was performed by searching the individual peak lists against a concatenated target-decoy database containing the *E. coli* sequences in the Uniprot database (release 2012_06) supplemented with a common contaminants database using the Mascot search engine version 2.3 (Matrix Science, London, United Kingdom) via the Proteome Discoverer interface. The search parameters included the use of trypsin as proteolytic enzyme allowing up to a maximum of 2 missed cleavages. Carbamidomethylation of cysteines was set as a fixed modification whereas oxidation of methionines were set as variable modifications. Precursor mass tolerance was initially set at 50 ppm, while fragment mass tolerance was set at 0.6 Da. Subsequently, the peptide identifications were filtered for an ion score of 20.

Fluorescence localization, immunolocalization, and related image analysis (related to Fig. 3 and S5-S8)

691 ***Bacterial strains and growth conditions for localization experiments***

692 Cells were grown to steady state in glucose minimal medium (GB1) pH 7.0 (den Blaauwen *et al.*, 1999)
693 supplemented with 50 µg/ml of required amino acids (LMC500 and derived strains) or 20 µg/ml thymine
694 (BW25113 and derived strains) at 28°C, or in Lennox LB medium pH 7.0 at 28°C, as indicated.
695 Absorbance was measured at 450 nm (GB1) or 600 nm (Lennox LB) with a Biochrom Libra S70.
696 Generation times of LMC500 strain grown in GB1 and Lennox LB medium at 28°C are 85 and 40 min,
697 respectively, and for BW25113 92 and 40 min, respectively.

698 ***Fluorescence localization of CpoB-mCherry and GFPmut2-TolA***

699 *mCherry* was placed in frame after the endogenous *cpoB* gene in the chromosome of *E. coli* MC4100
700 (LMC500); *gfpmut2* was placed in frame before the *tolA* gene (see Bacterial strains and plasmids,
701 above). Cells were grown to steady state in glucose minimal medium at 28°C, then placed on a 0.5 x
702 0.5 cm 1% agarose patch (Koppelman *et al.*, 2004) containing minimal medium on an object glass to
703 allow for optimal aeration, covered by a cover glass and immediately imaged as described (van der
704 Ploeg *et al.*, 2013). Images were acquired with Micro-Manager (<http://www.micro-manager.org/>) with
705 direct output of the desired hyperstack structure for ImageJ by Wayne Rasband
706 (<http://imagej.nih.gov/ij/>). CpoB-mcherry was used because the localization of freely diffusing
707 periplasmic proteins was observed to be perturbed by fixation, likely due to osmotic effects. GFP-TolA
708 was used because available antiserum was not useable for immunolabeling. Both fusions were
709 functional (Fig. S4).

710 **Immunolocalization**

711 *E. coli* cells of wild type strain LMC500 were grown to steady state in glucose minimal medium at 28°C,
712 then fixed while shaking in growth medium as described (den Blaauwen *et al.*, 2003). Cells were
713 permeabilized and immunolabelled with indicated antibodies as described (den Blaauwen *et al.*, 2003),
714 immobilized on 1% agarose and imaged as above. Bodipy-12, a membrane binding dye, was used as a
715 control to show at what stage constriction results in increased mid-cell fluorescence due to the
716 presence of two membranes. Antisera against PBP1B and LpoB were affinity purified and pre-
717 incubated with cells of their respective deletion strains before use in immunolabeling. Antisera against
718 FtsZ and FtsN were specific without further purification. The immunolabeling method used here has
719 been shown to be reproducible and to not perturb the localization of membrane and cytoplasmic and
720 proteins (van der Ploeg *et al.*, 2013).

721 **Related image analysis**

722 Image analysis was performed as described (van der Ploeg *et al.*, 2013). Briefly, individual cells were
723 identified and analyzed using the public domain program Coli-Inspector, running under plugin ObjectJ
724 written by Norbert Vischer (University of Amsterdam, <http://simon.bio.uva.nl/objectj/>), which runs in
725 combination with ImageJ. Via this analysis, parameters including cell length, cell diameter (width) as a
726 function of length, and integrated fluorescence as a function of length (fluorescence profile) were
727 quantified for each cell. For each examined protein, fluorescence profiles of 3000-5000 individual cells
728 were sorted according to cell length to generate profile maps (Fig. 3B), similar to demographs (Hocking

729 *et al.*, 2012). A cell diameter profile map (Fig. 3B, bottom panel) was generated from imaged cells that
730 were fixed only. % cell cycle progression (age) for individual cells was determined based on relative cell
731 length ranking, assuming a logarithmic growth of cell length (Aarsman *et al.*, 2005). Average
732 fluorescence profiles for either all cells or specific age ranges were generated and plotted against
733 normalized cell length as described (Potluri *et al.*, 2010) (Fig. 3C). Cell ages corresponding to the
734 initiation of mid-cell localization and peak mid-cell localization for each examined protein (Fig. 3D) were
735 determined as described in Fig. S6 and below.

736 ***CpoB immunolocalization and related image analysis*** (related to Fig. S5, S7 and S8)

737 To examine cell division protein dependencies for CpoB mid-cell localization (Fig. S7), isogenic
738 strains based on the parental strain LMC500 (see Bacterial Strains and Plasmids, above) with
739 temperature-sensitive alleles of cell division proteins (Taschner *et al.*, 1988) were used. Cells were
740 grown in glucose minimal medium at 28°C (permissive temperature) to an OD₄₅₀ of 0.2. Subsequently,
741 the growing cells were diluted 1:4 into pre-warmed medium of 28°C or 42°C and grown until the
742 cultures again reached an OD₄₅₀ of 0.2. Cells were fixed, permeabilized and immunolabeled as
743 described (Methods and (den Blaauwen *et al.*, 2003)) using antibody to CpoB that had been pre-
744 adsorbed on permeabilized $\Delta cpoB$ cells to remove cross-reacting antibodies, as described previously
745 (Buddelmeijer *et al.*, 2013). Cells were sorted according to length to generate fluorescence profile maps,
746 as described in Methods (~500-1000 cells per profile). The FtsZ(ts) strain LMC509 (Taschner *et al.*,
747 1988) is not completely temperature sensitive; consequently, CpoB still localizes at mid-cell in shorter

748 cells in this strain; however, in long smooth cells, no mid-cell localization is seen. The PBP3(ts) strain
749 LMC510 (Taschner *et al.*, 1988) is already somewhat elongated at the permissive temperature due to
750 the presence of an unstable PBP3 molecule (Fraipont *et al.*, 2011). The FtsW(ts) strain JLB17 is not
751 isogenic to LMC500 (Mohammadi *et al.*, 2014, Ishino *et al.*, 1989) and was grown in Lennox LB
752 medium without salt and with 1% glucose and 20 mg/mL of thymine at 28°C to an OD₆₀₀ of 0.3. Strain
753 JOE565 (FtsN depletion) (Chen and Beckwith, 2001) was grown in Lennox LB with 0.2% arabinose at
754 28°C to an OD₆₀₀ of 0.3. Cells were washed in warm medium without arabinose and resuspended in
755 medium without arabinose to deplete FtsN. For aztreonam treatment (inhibits PBP3), LMC500 was
756 grown in glucose minimal medium at 28°C to an OD₄₅₀ of 0.2. The culture was then split diluted 1:4 into
757 medium with or without 2 µg/mL aztreonam and grown for an additional two mass doublings.

758 To examine dependency on PBP1B or TolA for CpoB mid-cell localization (Fig. S8), wild type
759 strain BW25113 and isogenic derivatives lacking *mrcB* or *tolA* were used. Cells were grown in Lennox
760 LB medium at 28°C to an OD₆₀₀ of 0.3, diluted 1:25 into pre-warmed medium and grown until the
761 cultures again reached an OD₆₀₀ of 0.3, then fixed, Immunolabeled with antibody to CpoB and imaged
762 as described above. Cells were sorted according to length to generate fluorescence profile maps, as
763 described in Methods (~1500 cells per profile). The $\Delta tolA$ strain had increased CpoB
764 immunofluorescence levels, with accumulation at constriction sites (Fig. S8B, middle two panels); TolA
765 overexpression (pTolA; see Bacterial Strains and Plasmids) alleviated this effect and reduced CpoB
766 immunofluorescence levels to below that of wild type (Fig. S8B, right two panels).

767 **Initiation and peak fluorescence localization** (related to Fig. S6)

768 Age of localization initiation was defined as the age class when extra mid-cell fluorescence was
769 first observed, as shown and described in Fig. S6. Age of peak localization was defined as the Moment
770 (Fig. S6B), i.e., the age when extra mid-cell fluorescence reached its maximum. For each analyzed cell
771 image, extra mid-cell fluorescence was calculated as 'FCplus' and plotted vs. cell age to determine the
772 Moment, as described (van der Ploeg *et al.*, 2013).

773

774 **In vitro protein interaction and activity assays** (related to Figs. 4, 5, S9 and S11)

775 SPR experiments were performed as previously described (Egan *et al.*, 2014). The concentration of
776 CpoB injected ranged from 0.05 to 0.5 μ M. Assays were performed in triplicate at 25°C, at a flow rate of
777 75 μ L/min and with an injection time of 5 min. The dissociation constant (K_D) was calculated by non-
778 linear regression using SigmaPlot 11 software (Systat software Inc., USA). Continuous fluorescence
779 GTase assays and measurement of TPase activity using radiolabelled lipid II substrate were performed
780 as described previously (Banzhaf *et al.*, 2012, Bertsche *et al.*, 2005).

781 **In vitro cross-linking – pulldown and non-reversed immunoblot approaches**

782 Proteins were mixed at appropriate concentrations in 200 μ L of binding buffer (10 mM HEPES/NaOH,
783 10 mM $MgCl_2$, 150 mM NaCl, 0.05% Triton X-100, pH 7.5). PBP1B or His-PBP1B at 1 μ M was used,
784 with 2 μ M LpoB(sol) or His-LpoB(sol), 1 μ M TolA or TolA-His and 4 μ M CpoB or His-CpoB where
785 indicated. Samples were incubated at room temperature for 10 min before addition of 0.2% w/v

786 formaldehyde (Sigma) and further incubation at 37°C for 10 min. Excess cross-linking was blocked by
787 addition of 100 mM Tris/HCl, pH 7.5. At this point the two approaches diverge. For the pulldown
788 approach samples were applied to 100 µL of washed and equilibrated Ni-NTA superflow beads
789 (QIAGEN) and incubated overnight at 4°C, with mixing. Beads were then washed with 6 × 1.5 mL wash
790 buffer (10 mM HEPES/NaOH, 10 mM MgCl₂, 500 mM NaCl, 50 mM imidazole, 0.05% Triton X-100, pH
791 7.5). Retained proteins were eluted by directly boiling beads in SDS-PAGE loading buffer, beads were
792 then removed and samples resolved by SDS-PAGE, gels were stained with coomassie brilliant blue
793 (Roth, Germany). For the non-reversed immunoblot approach samples were resolved by non-
794 denaturing 4 – 20% gradient SDS-PAGE and transferred to nitrocellulose membrane by western blot.
795 Proteins were identified using specific antibodies, detection was with ECL prime chemiluminescence
796 (GE Healthcare) imaged using an ImageQuant LAS4000mini (GE Healthcare).

797

798 ***In vivo* DTSSP cross-linking and co-immunoprecipitation assays** (related to Fig. 6)

799 Assays were performed as described (Bertsche *et al.*, 2006, Typas *et al.*, 2010) with minor
800 modifications: Cells were grown overnight, diluted 1:400 into 250 mL Lennox LB, and grown with
801 shaking in baffled flasks at 30°C to OD₆₀₀ = 0.3-0.4. Cells were then pelleted by centrifugation and
802 resuspended at a cell density equivalent to OD₆₀₀ = 10 in ice-cold CL Buffer I (50 mM NaH₂PO₄ 20%
803 (w/v) sucrose pH 7.4) with 100 µg/mL DTSSP (freshly prepared as a 20 mg/mL stock in CL Buffer I).
804 Cells were incubated at 4°C with mixing for 1 h, then pelleted and frozen at -80°C. Cells were then

805 thawed, resuspended at OD600 = 4 in ice-cold CL Buffer II (100 mM Tris-HCl 10 mM MgCl₂, 1 M NaCl
806 pH 7.5) with 100 µM PMSF, 50 µg/ml protease inhibitor cocktail (Sigma P8465) and 50 µg/ml DNase I,
807 and lysed using a microfluidizer. Otherwise, method was as described in (Bertsche *et al.*, 2006, Typas
808 *et al.*, 2010).

809

810 **Data-driven structural docking models** (related to Fig. 7A)

811 The docking models of CpoB/PBP1B/LpoB complex were built using HADDOCK2.1 data-driven
812 docking protocols (Dominguez *et al.*, 2003) and CNS1.2 (Brunger *et al.*, 1998) for the structure
813 calculations. The initial coordinates of the CpoB, PBP1B and LpoB molecules were taken from the
814 PBP1B crystal structure (PDB code 3VMA) (Sung *et al.*, 2009), the CpoB crystal structure from the N-
815 terminal domain (2XDJ) and the C-terminal TPR domain (2XEV) (Krachler *et al.*, 2010) and from the
816 LpoB NMR structure (2MII) (Egan *et al.*, 2014). During the multi-body docking, ambiguous restraints
817 were applied to drive the docking according to the different experimental data. For LpoB, ambiguous
818 interaction restraints were defined based on the NMR chemical shift perturbation mapping recorded
819 on the LpoB/UB2H complex and on the *in vivo* and *in vitro* activities of LpoB and PBP1B alleles as
820 described in (Egan *et al.*, 2014). For CpoB, *in vivo* cross-linking detected using *pBpa* substitutions at
821 PBP1B residues 118, 123, 751 and 753 were used as active restraints to drive the interaction between
822 PBP1B and CpoB. Due to the absence of a unique structure of the disordered N-terminal domain of

823 LpoB (residues 1-60) and the linker between the N- and C-terminal domains of CpoB (residues 91-108),
824 the two regions were treated as fully flexible.

825 The docking was performed with default HADDOCK parameters including a clustering cutoff of
826 7.5 Å. The HADDOCK score was used to rank the generated models (Lutje Hulsik *et al.*, 2013). The
827 generated docking models were analyzed within the Pymol software.

828

829 **Chlorophenyl red-β-D-galactopyranoside (CPRG) penetration assay** (related to Fig. S1A-B)

830 The CPRG assay was performed as described (Paradis-Bleau *et al.*, 2014) with slight
831 modifications. Instead of normal rectangular agar plates in which colonies are arrayed next to each
832 other and color can diffuse, we used 384-well plates, filled with LB-agar-CPRG by a liquid handling
833 robot (Biomek FX, Beckman Coulter). Mutants carrying pCB112, a mobile plasmid encoding *lacZ* under
834 control of the lactose promoter (P_{lac}) were arrayed robotically on each well (Singer ROTOR). Color
835 development (CPR-red; 570nm) was monitored for 48 hours (every 30 min) in multi-well plate reader
836 (Tecan M1000 Pro with a stacker) at room temperature. Absorption wavelength (not to overlap with
837 colony development), agar volume per well and a number of other technical parameters were optimized
838 for the assay (George Kritikos and Athanasios Typas; unpublished data). The accumulation rate of
839 CPR color was calculated after fitting a linear curve on absorption-time plot.

840

841 **Filtered culture supernatants** (related to Fig. S1C)

842 Culture supernatants collected and filtered using a 0.2 µm-pore SFCA syringe filter (Fisher),
843 then TCA-precipitated and prepared for analysis by SDS-PAGE and western blot as described (Wagner
844 *et al.*, 2009).

845

846 **Determination of CpoB copy number** (related to Fig. S10)

847 BW25113 and BW25113 $\Delta cpoB$ were grown in 50 mL of LB to an OD₅₇₈ of 0.3. The culture
848 was then back-diluted 1 in 50 into 50 mL fresh LB and grown to an OD₅₇₈ of 0.3. Cells were then
849 cooled on ice for 10 min prior to harvesting of 5 mL by centrifugation (10000 × g, 10 min, 4°C). At this
850 point a viable count was also performed to determine the number of cells per ml of culture (see below).
851 The pellets were resuspended in 100 µL TBS (Tris-buffered saline) buffer and lysed by addition of 100
852 µL SDS-PAGE loading buffer and boiling for 10 min. 3 × 20 µL samples of BW25113 lysate were
853 resolved by SDS-PAGE along with purified CpoB standards (0, 1, 2, 4, 8 and 16 ng) loaded in 20 µL of
854 BW25113 $\Delta cpoB$ lysate. CpoB was detected with specific antibody after western blot (Fig. S10).
855 Images were analysed using ImageQuant LAS4000 software, giving the chemiluminescence signal
856 derived from CpoB bands over the background (the signal at the same position as CpoB in the 0 ng
857 sample was used as the background). A standard curve was plotted using the known CpoB standards
858 and the amount of CpoB in the BW25113 lysate samples was calculated. This was then converted to
859 molecules per cell using the viable counts, which were performed as follows. Cells were serially diluted
860 10-fold in ice-cold LB. 100 µl of the 10⁻⁵ and 10⁻⁶ dilutions were plated on LB agar and grown overnight

861 at 37°C, the number of colonies were then counted and the number of cells per ml of culture was
862 calculated.

863 **ACKNOWLEDGEMENTS**

864

865 We thank Adeline Derouaux and Tom Bernhardt for reagents and strains. We thank Monica Guo and
866 Jason Peters for critical reading of the manuscript. This work was supported by: the Wellcome Trust
867 [101824/Z/13/Z] (to W.V.); the National Institutes of Health (NIH) [5RO1GM102790] (to C.A.G.),
868 [1P50GM107615-01] (to K.C.H.); the Alexander von Humboldt Foundation Sofja Kovalevskaja Award
869 (to A.T.); European Molecular Biology Laboratory internal funding (to A.T.); the European Commission
870 DIVINOCELL project [FP7-Health-2007-B-223431] (to T.d.B.); the Council for Chemical Sciences of
871 The Netherlands - Organization for Scientific Research (CWNWO) [ECHO-project # 700.59.005] (to
872 E.B); the National Science Foundation (NSF) CAREER Award [MCB-1149328] (to K.C.H.); and a
873 Stanford Graduate Fellowship (to A.C.).

874

875 **REFERENCES**

- 876 Aarsman, M. E., Piette, A., Fraipont, C., Vinkenvleugel, T. M., Nguyen-Disteche, M. & den Blaauwen, T.
877 2005. Maturation of the Escherichia coli divisome occurs in two steps. *Mol Microbiol* **55**:1631-45.
878 doi:10.1111/j.1365-2958.2005.04502.x.
- 879 Baba, T., Ara, T., Hasegawa, M., Takai, Y., Okumura, Y., Baba, M., Datsenko, K. A., Tomita, M.,
880 Wanner, B. L. & Mori, H. 2006. Construction of Escherichia coli K-12 in-frame, single-gene
881 knockout mutants: the Keio collection. *Mol Syst Biol* **2**:2006 0008. doi:10.1038/msb4100050.
- 882 Banzhaf, M., van den Berg van Saparoea, B., Terrak, M., Fraipont, C., Egan, A., Philippe, J., Zapun, A.,
883 Breukink, E., Nguyen-Disteche, M., den Blaauwen, T. & Vollmer, W. 2012. Cooperativity of
884 peptidoglycan synthases active in bacterial cell elongation. *Mol Microbiol* **85**:179-94.
885 doi:10.1111/j.1365-2958.2012.08103.x.
- 886 Bernadac, A., Gavioli, M., Lazzaroni, J. C., Raina, S. & Lloubes, R. 1998. *Escherichia coli* tol-pal
887 mutants form outer membrane vesicles. *J Bacteriol* **180**:4872-8. doi:not available.
- 888 Bertsche, U., Breukink, E., Kast, T. & Vollmer, W. 2005. In vitro murein peptidoglycan synthesis by
889 dimers of the bifunctional transglycosylase-transpeptidase PBP1B from Escherichia coli. *J Biol*
890 *Chem* **280**:38096-101. doi:10.1074/jbc.M508646200.
- 891 Bertsche, U., Kast, T., Wolf, B., Fraipont, C., Aarsman, M. E., Kannenberg, K., von Rechenberg, M.,
892 Nguyen-Disteche, M., den Blaauwen, T., Holtje, J. V. & Vollmer, W. 2006. Interaction between

893 two murein (peptidoglycan) synthases, PBP3 and PBP1B, in *Escherichia coli*. *Mol Microbiol*
 894 **61**:675-90. doi:10.1111/j.1365-2958.2006.05280.x.

895 Bi, E. F. & Lutkenhaus, J. 1991. FtsZ ring structure associated with division in *Escherichia coli*. *Nature*
 896 **354**:161-4. doi:10.1038/354161a0.

897 Blomfield, I. C., Vaughn, V., Rest, R. F. & Eisenstein, B. I. 1991. Allelic exchange in *Escherichia coli*
 898 using the *Bacillus subtilis* sacB gene and a temperature-sensitive pSC101 replicon. *Mol*
 899 *Microbiol* **5**:1447-57. doi:10.1111/j.1365-2958.1991.tb00791.x.

900 Born, P., Breukink, E. & Vollmer, W. 2006. In vitro synthesis of cross-linked murein and its attachment
 901 to sacculi by PBP1A from *Escherichia coli*. *J Biol Chem* **281**:26985-93.
 902 doi:10.1074/jbc.M604083200.

903 Breukink, E., van Heusden, H. E., Vollmerhaus, P. J., Swiezewska, E., Brunner, L., Walker, S., Heck, A.
 904 J. & de Kruijff, B. 2003. Lipid II is an intrinsic component of the pore induced by nisin in bacterial
 905 membranes. *J Biol Chem* **278**:19898-903. doi:10.1074/jbc.M301463200.

906 Brunger, A. T., Adams, P. D., Clore, G. M., DeLano, W. L., Gros, P., Grosse-Kunstleve, R. W., Jiang, J.
 907 S., Kuszewski, J., Nilges, M., Pannu, N. S., Read, R. J., Rice, L. M., Simonson, T. & Warren, G.
 908 L. 1998. Crystallography & NMR system: A new software suite for macromolecular structure
 909 determination. *Acta Crystallogr D Biol Crystallogr* **54**:905-21. doi:10.1107/S0907444498003254.

910 Buddelmeijer, N., Aarsman, M. & den Blaauwen, T. 2013. Immunolabeling of Proteins in situ in
 911 *Escherichia coli* K12 Strains. *Bio-protocol* **3**:e852. <http://www.bio-protocol.org/e852>.

912 Cascales, E., Bernadac, A., Gavioli, M., Lazzaroni, J. C. & Lloubes, R. 2002. Pal lipoprotein of
 913 *Escherichia coli* plays a major role in outer membrane integrity. *J Bacteriol* **184**:754-9.
 914 doi:10.1128/JB.184.3.754-759.2002.

915 Cascales, E., Gavioli, M., Sturgis, J. N. & Lloubes, R. 2000. Proton motive force drives the interaction of
 916 the inner membrane TolA and outer membrane pal proteins in *Escherichia coli*. *Mol Microbiol*
 917 **38**:904-15. doi:10.1046/j.1365-2958.2000.02190.x.

918 Cascales, E., Lloubes, R. & Sturgis, J. N. 2001. The TolQ-TolR proteins energize TolA and share
 919 homologies with the flagellar motor proteins MotA-MotB. *Mol Microbiol* **42**:795-807.
 920 doi:10.1046/j.1365-2958.2001.02673.x.

921 Chen, J. C. & Beckwith, J. 2001. FtsQ, FtsL and FtsI require FtsK, but not FtsN, for co-localization with
 922 FtsZ during *Escherichia coli* cell division. *Mol Microbiol* **42**:395-413. doi:10.1046/j.1365-
 923 2958.2001.02640.x.

924 Chin, J. W. & Schultz, P. G. 2002. In vivo photocrosslinking with unnatural amino Acid mutagenesis.
 925 *ChemBiochem* **3**:1135-7. doi:10.1002/1439-7633(20021104)3:11<1135::AID-
 926 CBIC1135>3.0.CO;2-M.

927 Cho, H., Uehara, T. & Bernhardt, T. G. 2014. Beta-lactam antibiotics induce a lethal malfunctioning of
 928 the bacterial cell wall synthesis machinery. *Cell* **159**:1300-11. doi:10.1016/j.cell.2014.11.017.

929 Datsenko, K. A. & Wanner, B. L. 2000. One-step inactivation of chromosomal genes in *Escherichia coli*
 930 K-12 using PCR products. *Proc Natl Acad Sci U S A* **97**:6640-5. doi:10.1073/pnas.120163297.

931 Datta, S., Costantino, N. & Court, D. L. 2006. A set of recombineering plasmids for gram-negative
 932 bacteria. *Gene* **379**:109-15. doi:10.1016/j.gene.2006.04.018.

933 de Vries, S. J., van Dijk, M. & Bonvin, A. M. 2010. The HADDOCK web server for data-driven
 934 biomolecular docking. *Nat Protoc* **5**:883-97. doi:10.1038/nprot.2010.32.

935 Demchick, P. & Koch, A. L. 1996. The permeability of the wall fabric of *Escherichia coli* and *Bacillus*
 936 *subtilis*. *J Bacteriol* **178**:768-73. doi:not available.

937 den Blaauwen, T., Aarsman, M. E., Vischer, N. O. & Nanninga, N. 2003. Penicillin-binding protein PBP2
 938 of *Escherichia coli* localizes preferentially in the lateral wall and at mid-cell in comparison with
 939 the old cell pole. *Mol Microbiol* **47**:539-47. doi:10.1046/j.1365-2958.2003.03316.x.

940 den Blaauwen, T., Buddelmeijer, N., Aarsman, M. E., Hameete, C. M. & Nanninga, N. 1999. Timing of
 941 FtsZ assembly in *Escherichia coli*. *J Bacteriol* **181**:5167-75. doi:not available.

942 Dominguez, C., Boelens, R. & Bonvin, A. M. 2003. HADDOCK: a protein-protein docking approach
 943 based on biochemical or biophysical information. *J Am Chem Soc* **125**:1731-7.
 944 doi:10.1021/ja026939x.

945 Dörr, T., Moll, A., Chao, M. C., Cava, F., Lam, H., Davis, B. M. & Waldor, M. K. 2014. Differential
 946 requirement for PBP1a and PBP1b in in vivo and in vitro fitness of *Vibrio cholerae*. *Infect Immun*
 947 **82**:2115-24. doi:10.1128/IAI.00012-14.

948 Edelstein, A., Amodaj, N., Hoover, K., Vale, R. & Stuurman, N. 2010. Computer control of microscopes
 949 using microManager. *Curr Protoc Mol Biol* **Chapter 14**:Unit14 20.
 950 doi:10.1002/0471142727.mb1420s92.

951 Egan, A. J., Jean, N. L., Koumoutsis, A., Bougault, C. M., Biboy, J., Sassine, J., Solovyova, A. S.,
 952 Breukink, E., Typas, A., Vollmer, W. & Simorre, J. P. 2014. Outer-membrane lipoprotein LpoB
 953 spans the periplasm to stimulate the peptidoglycan synthase PBP1B. *Proc Natl Acad Sci U S A*
 954 **111**:8197-202. doi:10.1073/pnas.1400376111.

955 Egan, A. J. F. & Vollmer, W. 2013. The physiology of bacterial cell division. *Ann N Y Acad Sci* **1277**:8-
 956 28. doi:10.1111/j.1749-6632.2012.06818.x.

957 Fraipont, C., Alexeeva, S., Wolf, B., van der Ploeg, R., Schloesser, M., den Blaauwen, T. & Nguyen-
 958 Disteché, M. 2011. The integral membrane FtsW protein and peptidoglycan synthase PBP3
 959 form a subcomplex in *Escherichia coli*. *Microbiology* **157**:251-9. doi:10.1099/mic.0.040071-0.

960 Fung, J., MacAlister, T. J. & Rothfield, L. I. 1978. Role of murein lipoprotein in morphogenesis of the
 961 bacterial division septum: phenotypic similarity of *lkyD* and *lpo* mutants. *J Bacteriol* **133**:1467-71.
 962 doi:not available.

963 Gan, L., Chen, S. & Jensen, G. J. 2008. Molecular organization of Gram-negative peptidoglycan. *Proc*
 964 *Natl Acad Sci U S A* **105**:18953-7. doi:10.1073/pnas.0808035105.

965 Garcia del Portillo, F. & de Pedro, M. A. 1990. Differential effect of mutational impairment of penicillin-
 966 binding proteins 1A and 1B on Escherichia coli strains harboring thermosensitive mutations in
 967 the cell division genes ftsA, ftsQ, ftsZ, and pbpB. *J Bacteriol* **172**:5863-70. doi:not available.

968 Gerding, M. A., Ogata, Y., Pecora, N. D., Niki, H. & de Boer, P. A. 2007. The trans-envelope Tol-Pal
 969 complex is part of the cell division machinery and required for proper outer-membrane
 970 invagination during cell constriction in E. coli. *Mol Microbiol* **63**:1008-25. doi:10.1111/j.1365-
 971 2958.2006.05571.x.

972 Germon, P., Ray, M. C., Vianney, A. & Lazzaroni, J. C. 2001. Energy-dependent conformational
 973 change in the TolA protein of Escherichia coli involves its N-terminal domain, TolQ, and TolR. *J*
 974 *Bacteriol* **183**:4110-4. doi:10.1128/JB.183.14.4110-4114.2001.

975 Guzman, L. M., Belin, D., Carson, M. J. & Beckwith, J. 1995. Tight regulation, modulation, and high-
 976 level expression by vectors containing the arabinose PBAD promoter. *J Bacteriol* **177**:4121-30.
 977 doi:not available.

978 Hantke, K. & Braun, V. 1973. Covalent binding of lipid to protein. Diglyceride and amide-linked fatty
 979 acid at the N-terminal end of the murein-lipoprotein of the Escherichia coli outer membrane. *Eur*
 980 *J Biochem* **34**:284-96. doi:10.1111/j.1432-1033.1973.tb02757.x.

981 Heckman, K. L. & Pease, L. R. 2007. Gene splicing and mutagenesis by PCR-driven overlap extension.
 982 *Nat Protoc* **2**:924-32. doi:10.1038/nprot.2007.132.

983 Heidrich, C., Templin, M. F., Ursinus, A., Merdanovic, M., Berger, J., Schwarz, H., de Pedro, M. A. &
 984 Holtje, J. V. 2001. Involvement of N-acetylmuramyl-L-alanine amidases in cell separation and
 985 antibiotic-induced autolysis of *Escherichia coli*. *Mol Microbiol* **41**:167-78. doi:10.1046/j.1365-
 986 2958.2001.02499.x.

987 Hocking, J., Priyadarshini, R., Takacs, C. N., Costa, T., Dye, N. A., Shapiro, L., Vollmer, W. & Jacobs-
 988 Wagner, C. 2012. Osmolality-dependent relocation of penicillin-binding protein PBP2 to the
 989 division site in *Caulobacter crescentus*. *J Bacteriol* **194**:3116-27. doi:10.1128/JB.00260-12.

990 Ishino, F., Jung, H. K., Ikeda, M., Doi, M., Wachi, M. & Matsushashi, M. 1989. New mutations *fts-36*, *fts-*
 991 *33*, and *ftsW* clustered in the *mra* region of the *Escherichia coli* chromosome induce
 992 thermosensitive cell growth and division. *J Bacteriol* **171**:5523-30. doi:not available.

993 Jean, N. L., Bougault, C. M., Lodge, A., Derouaux, A., Callens, G., Egan, A. J., Ayala, I., Lewis, R. J.,
 994 Vollmer, W. & Simorre, J. P. 2014. Elongated structure of the outer-membrane activator of
 995 peptidoglycan synthesis LpoA: implications for PBP1A stimulation. *Structure* **22**:1047-54.
 996 doi:10.1016/j.str.2014.04.017.

997 Kohlrausch, U. & Holtje, J. V. 1991. Analysis of murein and murein precursors during antibiotic-induced
 998 lysis of *Escherichia coli*. *J Bacteriol* **173**:3425-31. doi:not available.

999 Koppelman, C. M., Aarsman, M. E., Postmus, J., Pas, E., Muijsers, A. O., Scheffers, D. J., Nanninga, N.
 1000 & den Blaauwen, T. 2004. R174 of *Escherichia coli* FtsZ is involved in membrane interaction

1001 and protofilament bundling, and is essential for cell division. *Mol Microbiol* **51**:645-57.
 1002 doi:10.1046/j.1365-2958.2003.03876.x.
 1003 Krachler, A. M., Sharma, A., Cauldwell, A., Papadakos, G. & Kleanthous, C. 2010. TolA modulates the
 1004 oligomeric status of YbgF in the bacterial periplasm. *J Mol Biol* **403**:270-85.
 1005 doi:10.1016/j.jmb.2010.08.050.
 1006 Leisch, N., Verheul, J., Heindl, N. R., Gruber-Vodicka, H. R., Pende, N., den Blaauwen, T. & Bulgheresi,
 1007 S. 2012. Growth in width and FtsZ ring longitudinal positioning in a gammaproteobacterial
 1008 symbiont. *Curr Biol* **22**:R831-2. doi:10.1016/j.cub.2012.08.033.
 1009 Li, G. W., Burkhardt, D., Gross, C. & Weissman, J. S. 2014. Quantifying absolute protein synthesis
 1010 rates reveals principles underlying allocation of cellular resources. *Cell* **157**:624-35.
 1011 doi:10.1016/j.cell.2014.02.033.
 1012 Lloubes, R., Cascales, E., Walburger, A., Bouveret, E., Lazdunski, C., Bernadac, A. & Journet, L. 2001.
 1013 The Tol-Pal proteins of the Escherichia coli cell envelope: an energized system required for
 1014 outer membrane integrity? *Res Microbiol* **152**:523-9. doi:10.1016/S0923-2508(01)01226-8.
 1015 Loose, M. & Mitchison, T. J. 2014. The bacterial cell division proteins FtsA and FtsZ self-organize into
 1016 dynamic cytoskeletal patterns. *Nat Cell Biol* **16**:38-46. doi:10.1038/ncb2885.
 1017 Lupoli, T. J., Lebar, M. D., Markovski, M., Bernhardt, T., Kahne, D. & Walker, S. 2014. Lipoprotein
 1018 activators stimulate Escherichia coli penicillin-binding proteins by different mechanisms. *J Am*
 1019 *Chem Soc* **136**:52-5. doi:10.1021/ja410813j.

1020 Lutje Hulsik, D., Liu, Y. Y., Strokappe, N. M., Battella, S., El Khattabi, M., McCoy, L. E., Sabin, C., Hinz,
 1021 A., Hock, M., Macheboeuf, P., Bonvin, A. M., Langedijk, J. P., Davis, D., Forsman Quigley, A.,
 1022 Aasa-Chapman, M. M., Seaman, M. S., Ramos, A., Poignard, P., Favier, A., Simorre, J. P.,
 1023 Weiss, R. A., Verrips, C. T., Weissenhorn, W. & Rutten, L. 2013. A gp41 MPER-specific llama
 1024 VHH requires a hydrophobic CDR3 for neutralization but not for antigen recognition. *PLoS*
 1025 *Pathog* **9**:e1003202. doi:10.1371/journal.ppat.1003202.

1026 MacAlister, T. J., Cook, W. R., Weigand, R. & Rothfield, L. I. 1987. Membrane-murein attachment at the
 1027 leading edge of the division septum: a second membrane-murein structure associated with
 1028 morphogenesis of the gram-negative bacterial division septum. *J Bacteriol* **169**:3945-51. doi:not
 1029 available.

1030 Matias, V. R., Al-Amoudi, A., Dubochet, J. & Beveridge, T. J. 2003. Cryo-transmission electron
 1031 microscopy of frozen-hydrated sections of Escherichia coli and Pseudomonas aeruginosa. *J*
 1032 *Bacteriol* **185**:6112-8. doi:10.1128/JB.185.20.6112-6118.2003.

1033 Mohammadi, T., Sijbrandi, R., Lutters, M., Verheul, J., Martin, N. I., den Blaauwen, T., de Kruijff, B. &
 1034 Breukink, E. 2014. Specificity of the transport of lipid II by FtsW in Escherichia coli. *J Biol Chem*
 1035 **289**:14707-18. doi:10.1074/jbc.M114.557371.

1036 Muller, P., Ewers, C., Bertsche, U., Anstett, M., Kallis, T., Breukink, E., Fraipont, C., Terrak, M.,
 1037 Nguyen-Disteche, M. & Vollmer, W. 2007. The essential cell division protein FtsN interacts with

1038 the murein (peptidoglycan) synthase PBP1B in Escherichia coli. *J Biol Chem* **282**:36394-402.

1039 doi:10.1074/jbc.M706390200.

1040 Nesvizhskii, A. I., Keller, A., Kolker, E. & Aebersold, R. 2003. A statistical model for identifying proteins

1041 by tandem mass spectrometry. *Anal Chem* **75**:4646-58. doi:10.1021/ac0341261.

1042 Nichols, R. J., Sen, S., Choo, Y. J., Beltrao, P., Zietek, M., Chaba, R., Lee, S., Kazmierczak, K. M., Lee,

1043 K. J., Wong, A., Shales, M., Lovett, S., Winkler, M. E., Krogan, N. J., Typas, A. & Gross, C. A.

1044 2011. Phenotypic landscape of a bacterial cell. *Cell* **144**:143-56. doi:10.1016/j.cell.2010.11.052.

1045 Nikaido, H. 2003. Molecular basis of bacterial outer membrane permeability revisited. *Microbiol Mol Biol*

1046 *Rev* **67**:593-656. doi:10.1128/MMBR.67.4.593-656.2003.

1047 Nilsen, T., Ghosh, A. S., Goldberg, M. B. & Young, K. D. 2004. Branching sites and morphological

1048 abnormalities behave as ectopic poles in shape-defective Escherichia coli. *Mol Microbiol*

1049 **52**:1045-54. doi:10.1111/j.1365-2958.2004.04050.x.

1050 Obermann, W. & Holtje, J. V. 1994. Alterations of murein structure and of penicillin-binding proteins in

1051 minicells from Escherichia coli. *Microbiology* **140 (Pt 1)**:79-87. doi:10.1099/13500872-140-1-79.

1052 Osawa, M., Anderson, D. E. & Erickson, H. P. 2009. Curved FtsZ protofilaments generate bending

1053 forces on liposome membranes. *EMBO J* **28**:3476-84. doi:10.1038/emboj.2009.277.

1054 Osawa, M. & Erickson, H. P. 2013. Liposome division by a simple bacterial division machinery. *Proc*

1055 *Natl Acad Sci U S A* **110**:11000-4. doi:10.1073/pnas.1222254110.

1056 Paradis-Bleau, C., Kritikos, G., Orlova, K., Typas, A. & Bernhardt, T. G. 2014. A genome-wide screen
 1057 for bacterial envelope biogenesis mutants identifies a novel factor involved in cell wall precursor
 1058 metabolism. *PLoS Genet* **10**:e1004056. doi:10.1371/journal.pgen.1004056.

1059 Paradis-Bleau, C., Markovski, M., Uehara, T., Lupoli, T. J., Walker, S., Kahne, D. E. & Bernhardt, T. G.
 1060 2010. Lipoprotein cofactors located in the outer membrane activate bacterial cell wall
 1061 polymerases. *Cell* **143**:1110-20. doi:10.1016/j.cell.2010.11.037.

1062 Parsons, L. M., Lin, F. & Orban, J. 2006. Peptidoglycan recognition by Pal, an outer membrane
 1063 lipoprotein. *Biochemistry* **45**:2122-8. doi:10.1021/bi052227i.

1064 Philippe, N., Alcaraz, J. P., Coursange, E., Geiselmann, J. & Schneider, D. 2004. Improvement of
 1065 pCVD442, a suicide plasmid for gene allele exchange in bacteria. *Plasmid* **51**:246-55.
 1066 doi:10.1016/j.plasmid.2004.02.003.

1067 Potluri, L., Karczmarek, A., Verheul, J., Piette, A., Wilkin, J. M., Werth, N., Banzhaf, M., Vollmer, W.,
 1068 Young, K. D., Nguyen-Disteche, M. & den Blaauwen, T. 2010. Septal and lateral wall
 1069 localization of PBP5, the major D,D-carboxypeptidase of Escherichia coli, requires substrate
 1070 recognition and membrane attachment. *Mol Microbiol* **77**:300-23. doi:10.1111/j.1365-
 1071 2958.2010.07205.x.

1072 Radolf, J. D., Caimano, M. J., Stevenson, B. & Hu, L. T. 2012. Of ticks, mice and men: understanding
 1073 the dual-host lifestyle of Lyme disease spirochaetes. *Nat Rev Microbiol* **10**:87-99.
 1074 doi:10.1038/nrmicro2714.

1075 Ryu, Y. & Schultz, P. G. 2006. Efficient incorporation of unnatural amino acids into proteins in
1076 *Escherichia coli*. *Nat Methods* **3**:263-5. doi:10.1038/nmeth864.

1077 Schneider, T. & Sahl, H. G. 2010. An oldie but a goodie - cell wall biosynthesis as antibiotic target
1078 pathway. *Int J Med Microbiol* **300**:161-9. doi:10.1016/j.ijmm.2009.10.005.

1079 Shevchenko, A., Tomas, H., Havlis, J., Olsen, J. V. & Mann, M. 2006. In-gel digestion for mass
1080 spectrometric characterization of proteins and proteomes. *Nat Protoc* **1**:2856-60.
1081 doi:10.1038/nprot.2006.468.

1082 Sung, M. T., Lai, Y. T., Huang, C. Y., Chou, L. Y., Shih, H. W., Cheng, W. C., Wong, C. H. & Ma, C.
1083 2009. Crystal structure of the membrane-bound bifunctional transglycosylase PBP1b from
1084 *Escherichia coli*. *Proc Natl Acad Sci U S A* **106**:8824-9. doi:10.1073/pnas.0904030106.

1085 Szwedziak, P., Wang, Q., Bharat, T. A., Tsim, M. & Löwe, J. 2014. Architecture of the ring formed by
1086 the tubulin homologue FtsZ in bacterial cell division. *Elife* **3**. doi:10.7554/eLife.04601.

1087 Szwedziak, P., Wang, Q., Freund, S. M. & Löwe, J. 2012. FtsA forms actin-like protofilaments. *EMBO J*
1088 **31**:2249-60. doi:10.1038/emboj.2012.76.

1089 Taschner, P. E., Huls, P. G., Pas, E. & Woldringh, C. L. 1988. Division behavior and shape changes in
1090 isogenic ftsZ, ftsQ, ftsA, pbpB, and ftsE cell division mutants of *Escherichia coli* during
1091 temperature shift experiments. *J Bacteriol* **170**:1533-40. doi:not available.

1092 Terrak, M., Ghosh, T. K., van Heijenoort, J., Van Beeumen, J., Lampilas, M., Aszodi, J., Ayala, J. A.,
1093 Ghuysen, J. M. & Nguyen-Disteche, M. 1999. The catalytic, glycosyl transferase and acyl

1094 transferase modules of the cell wall peptidoglycan-polymerizing penicillin-binding protein 1b of
 1095 Escherichia coli. *Mol Microbiol* **34**:350-64. doi:10.1046/j.1365-2958.1999.01612.x.
 1096 Thomason, L. C., Costantino, N. & Court, D. L. 2007. E. coli genome manipulation by P1 transduction.
 1097 *Curr Protoc Mol Biol* **Chapter 1**:Unit 1 17. doi:10.1002/0471142727.mb0117s79.
 1098 Thomason, L. C., Sawitzke, J. A., Li, X., Costantino, N. & Court, D. L. 2014. Recombineering: genetic
 1099 engineering in bacteria using homologous recombination. *Curr Protoc Mol Biol* **106**:1 16 1-1 16
 1100 39. doi:10.1002/0471142727.mb0116s106.
 1101 Typas, A., Banzhaf, M., Gross, C. A. & Vollmer, W. 2012. From the regulation of peptidoglycan
 1102 synthesis to bacterial growth and morphology. *Nat Rev Microbiol* **10**:123-36.
 1103 doi:10.1038/nrmicro2677.
 1104 Typas, A., Banzhaf, M., van den Berg van Saparoea, B., Verheul, J., Biboy, J., Nichols, R. J., Zietek, M.,
 1105 Beilharz, K., Kannenberg, K., von Rechenberg, M., Breukink, E., den Blaauwen, T., Gross, C. A.
 1106 & Vollmer, W. 2010. Regulation of peptidoglycan synthesis by outer-membrane proteins. *Cell*
 1107 **143**:1097-109. doi:10.1016/j.cell.2010.11.038.
 1108 Uehara, T., Dinh, T. & Bernhardt, T. G. 2009. LytM-domain factors are required for daughter cell
 1109 separation and rapid ampicillin-induced lysis in Escherichia coli. *J Bacteriol* **191**:5094-107.
 1110 doi:10.1128/JB.00505-09.
 1111 Uehara, T., Parzych, K. R., Dinh, T. & Bernhardt, T. G. 2010. Daughter cell separation is controlled by
 1112 cytokinetic ring-activated cell wall hydrolysis. *EMBO J* **29**:1412-22. doi:10.1038/emboj.2010.36.

l1113 Ursell, T. S., Nguyen, J., Monds, R. D., Colavin, A., Billings, G., Ouzounov, N., Gitai, Z., Shaevitz, J. W.
 l1114 & Huang, K. C. 2014. Rod-like bacterial shape is maintained by feedback between cell
 l1115 curvature and cytoskeletal localization. *Proc Natl Acad Sci U S A* **111**:E1025-34.
 l1116 doi:10.1073/pnas.1317174111.
 l1117 van der Ploeg, R., Verheul, J., Vischer, N. O., Alexeeva, S., Hoogendoorn, E., Postma, M., Banzhaf, M.,
 l1118 Vollmer, W. & den Blaauwen, T. 2013. Colocalization and interaction between elongasome and
 l1119 divisome during a preparative cell division phase in Escherichia coli. *Mol Microbiol* **87**:1074-87.
 l1120 doi:10.1111/mmi.12150.
 l1121 Vazquez-Laslop, N., Lee, H., Hu, R. & Neyfakh, A. A. 2001. Molecular sieve mechanism of selective
 l1122 release of cytoplasmic proteins by osmotically shocked Escherichia coli. *J Bacteriol* **183**:2399-
 l1123 404. doi:10.1128/JB.183.8.2399-2404.2001.
 l1124 Vianney, A., Muller, M. M., Clavel, T., Lazzaroni, J. C., Portalier, R. & Webster, R. E. 1996.
 l1125 Characterization of the tol-pal region of Escherichia coli K-12: translational control of tolR
 l1126 expression by TolQ and identification of a new open reading frame downstream of pal encoding
 l1127 a periplasmic protein. *J Bacteriol* **178**:4031-8. doi:not available.
 l1128 Vollmer, W., Blanot, D. & de Pedro, M. A. 2008. Peptidoglycan structure and architecture. *FEMS*
 l1129 *Microbiol Rev* **32**:149-167. doi:10.1111/j.1574-6976.2007.00094.x.

l130 Vollmer, W., von Rechenberg, M. & Holtje, J. V. 1999. Demonstration of molecular interactions between
 l131 the murein polymerase PBP1B, the lytic transglycosylase MltA, and the scaffolding protein MipA
 l132 of *Escherichia coli*. *J Biol Chem* **274**:6726-34. doi:10.1074/jbc.274.10.6726.
 l133 Wagner, J. K., Heindl, J. E., Gray, A. N., Jain, S. & Goldberg, M. B. 2009. Contribution of the
 l134 periplasmic chaperone Skp to efficient presentation of the autotransporter IcsA on the surface of
 l135 *Shigella flexneri*. *J Bacteriol* **191**:815-21. doi:10.1128/JB.00989-08.
 l136 Weigand, R. A., Vinci, K. D. & Rothfield, L. I. 1976. Morphogenesis of the bacterial division septum: a
 l137 new class of septation-defective mutants. *Proc Natl Acad Sci U S A* **73**:1882-6.
 l138 doi:10.1073/pnas.73.6.1882.
 l139 Weiss, D. S. 2015. Last but not least: new insights into how FtsN triggers constriction during
 l140 *Escherichia coli* cell division. *Mol Microbiol*. doi:10.1111/mmi.12925.
 l141 Yang, D. C., Peters, N. T., Parzych, K. R., Uehara, T., Markovski, M. & Bernhardt, T. G. 2011. An ATP-
 l142 binding cassette transporter-like complex governs cell-wall hydrolysis at the bacterial cytokinetic
 l143 ring. *Proc Natl Acad Sci U S A* **108**:E1052-60. doi:10.1073/pnas.1107780108.
 l144 Yousif, S. Y., Broome-Smith, J. K. & Spratt, B. G. 1985. Lysis of *Escherichia coli* by beta-lactam
 l145 antibiotics: deletion analysis of the role of penicillin-binding proteins 1A and 1B. *J Gen Microbiol*
 l146 **131**:2839-45. doi:not available.
 l147

1148 **FIGURE LEGENDS**

1149

1150 **Figure 1. Shared chemical sensitivities and genetic interactions implicate CpoB in PBP1B**
1151 **function.**

1152 **A.** Chemical genetic phenotype profiles for strains lacking PBP1B (encoded by *mrcB*), LpoB, and CpoB,
1153 from hierarchical clustering of the growth fitness of 3979 gene deletions across 324 chemical stress
1154 conditions (Nichols *et al.*, 2011). Blue, low fitness (sensitivity); yellow, high fitness (resistance). $\Delta mrcB$
1155 and $\Delta cpoB$ ($\Delta ybgF$) showed significant similarity. Underlined regions correspond to strongest shared
1156 sensitivities and are magnified below the full profile. **B.** Sensitivity of $\Delta cpoB$ to cefsulodin,
1157 predominantly an inhibitor of PBP1A, is alleviated by PBP1B overexpression. Growth fitness was
1158 assessed by pinning cells to agar plates in a 1536-spot format and quantifying colony size after 12-14 h
1159 of growth. Error bars depict standard deviations ($n \geq 44$). **C.** CpoB-associated envelope defects
1160 visualized by fluorescence microscopy using periplasmic mCherry. Arrowheads, fluorescent foci
1161 indicating OM blebs or vesicles; outlines, loss of peripheral fluorescence due to periplasmic leakage. **D-**
1162 **E.** Quantification of microscopy phenotypes: OM blebbing (**D**) and loss of periplasmic fluorescence (**E**),
1163 indicative of periplasmic leakage. Threshold value was established based on quantification of cells with
1164 known severe OM defects ($\Delta tolA$). Cells lacking CpoB exhibit envelope defects that were severely
1165 exacerbated in the absence of LpoA and alleviated by PBP1B overexpression. **F.** Quantification of

l166 growth fitness for indicated mutant strains. A strain lacking CpoB and LpoA exhibited a synthetic growth
l167 defect that was alleviated by PBP1B overexpression.

l168

l169 **Figure 2. PBP1B interacts with CpoB *in vivo*.**

l170 **A.** Photo-cross-linkable amino acid (*pBpa*) substitutions at the indicated positions in His6-PBP1B, lining
l171 a cleft between the TPase and UB2H domains, formed similar UV cross-linking products *in vivo*. **B.**
l172 SDS-PAGE and α -His6 immunoblot analysis revealed a cross-linked adduct ~120 kDa in size (MW of
l173 PBP1By = 88.9 kDa). Analysis of the products by MS revealed the presence of CpoB (MW = 28.2 kDa)
l174 cross-linked to PBP1B at each indicated position.

l175

l176 **Figure 3. CpoB localizes to mid-cell concurrent with PBP1B, TolA, and the onset of OM**
l177 **constriction.**

l178 **A.** Endogenously expressed CpoB-mCherry localizes to mid-cell during cell division. Left, phase
l179 contrast image; right, mCherry fluorescence; scale bar, 2 μ m. **B.** Localization of CpoB-mCherry as a
l180 function of cell cycle progression (cell length), with comparison to other proteins. PBP1B, LpoB, FtsZ,
l181 PBP3, and FtsN were visualized by immunofluorescence using specific antibodies. Cell membranes
l182 were stained with Bodipy-12. Cell width (diameter) was measured from phase contrast images.
l183 Constant brightness along the length of the cell indicates constant diameter; darkening at mid-cell in
l184 longer cells is indicative of constriction. To generate profile maps for each protein, fluorescence

intensity profiles (integrated fluorescence as a function of cell length) were derived for >1000 individual cell images and sorted vertically by cell length. Each horizontal line corresponds to a single cell. Y-axis scale indicates % cell-cycle progression based on cell length. Data for FtsZ, PBP3, FtsN, and cell width have been previously published (van der Ploeg *et al.*, 2013) and are used here for comparisons. **C.** Average distribution of CpoB-mCherry for different cell-cycle progression age groups. Fluorescence intensity profiles were normalized by length, then averaged and normalized to the peak local brightness for each age group. **D.** Relative timing of mid-cell recruitment for each examined protein. Initiation is based on the onset of enriched localization at mid-cell (quantified in Fig. S6A-B and (van der Ploeg *et al.*, 2013)). Peak is the point in the division cycle when maximal localization is reached.

1194

Figure 4. PBP1B interacts directly with CpoB and TolA.

A. CpoB interacts directly with PBP1B *in vitro*, assayed by SPR. Sensorgrams show binding of CpoB to a chip surface with immobilized PBP1B, but not PBP1A or an empty control surface. Concentrations of CpoB (0-0.5 μ M) are indicated. **B.** The K_D of the PBP1B-CpoB interaction was determined by non-linear regression using Sigma Plot 11.0. **C.** TolA interacts directly with PBP1B *in vitro* only when TolA contains its transmembrane domain I. Interaction between His6-PBP1B and either full length TolA or TolA(sol), a soluble variant lacking domain I, was assessed using an *in vitro* cross-linking/pull-down approach. His-PBP1B specifically retained TolA, but not the soluble version lacking domain I, when pulled down by Ni-NTA beads. TolA or TolA(sol) alone showed no significant binding to Ni-NTA.

1204

1205 **Figure 5. CpoB modulates stimulation of PBP1B TPase activity by LpoB.**

1206 GTase and TPase activities of PBP1B in the presence of LpoB, TolA, and/or CpoB. **A.** GTase rate was
1207 assayed by consumption of fluorescently labelled lipid II by PBP1B *in vitro*. Change in GTase rate is
1208 relative to PBP1B alone and is shown as mean \pm SD ($n = 3-4$). **B.** TPase activity was determined by
1209 analyzing peptide cross-linkage following *in vitro* PG synthesis by PBP1B with radiolabelled lipid II
1210 substrate. TPase activity is shown as % of peptides present in cross-links in PG produced by PBP1B
1211 (mean \pm SD). TPase assays were performed at 150 mM NaCl ($n = 4-7$) and at an increased salt
1212 concentration of 215 mM NaCl ($n = 2$, shown as the mean \pm maximum and minimum values), at which
1213 the negative impact of CpoB on PBP1B TPase stimulation by LpoB is exacerbated. Statistical
1214 significance/difference was determined by Mann-Whitney U test, with p values of 0.00058 for both data sets.

1215

1216 **Figure 6. Regulatory interactions between CpoB, TolA, and PBP1B-LpoB respond to Tol-Pal**

1217 **assembly and energy state.**

1218 **A-B.** Interactions between CpoB, TolA, PBP1B, and LpoB were characterized *in vivo* by cross-linking
1219 and co-immunoprecipitation for wild type (WT) and indicated mutant strains. Antibodies specific for
1220 CpoB, TolA, and PBP1B were used to immunoprecipitate their antigens from *E. coli* membrane extracts
1221 derived from cells treated with DTSSP cross-linker. Interacting proteins were detected in the immuno-

precipitates by western blot using specific antibodies. **C.** Schematic of observed *in vivo* interactions.

Black bars indicate interactions observed in WT; red bars indicate novel interactions in mutant strains.

Figure 7. Model for physical and functional coordination of the PBPB-LpoB PG synthesis and Tol-Pal OM constriction machines by CpoB.

A. Data-driven docking of the PBP1B/LpoB/CpoB complex calculated with HADDOCK/CNS protocols (de Vries *et al.*, 2010) and integrating experimental data. The lowest energy structure obtained is shown with PBP1B, LpoB, and CpoB colored in wheat, pale green, and blue, respectively. LpoB binds the PBP1B UB2H domain, while CpoB binds in an adjacent cleft between the UB2H and TPase domains (Fig. 2). We propose that CpoB can contact LpoB in this conformation, preventing hyper-activation of the PBP1B TPase by LpoB. TolA counteracts this CpoB effect, and increases both cross-linking (via LpoB) and GTase (directly) activities of PBP1B. **B.** Schematic of PBP1B regulation by LpoB, CpoB and Tol-Pal. TP, transpeptidase domain; GT, glycosyltransferase domain. Green circles indicate activity stimulation (increase in glycan synthesis rate for GTase; formation of higher cross-linked product for TPase). Top left: LpoB binding stimulates both PBP1B GTase and TPase activities; the latter produces a highly cross-linked PG. Top right: CpoB modulates TPase without interfering with GTase. Bottom left and right: When energized, TolA reverses the CpoB effect, restoring production of highly cross-linked PG. Regulation by TolA is thus dependent on Tol-Pal PMF utilization, tying cycles of PBP1B TPase activation to cycles of Tol-Pal activity.

Supplemental Figure S1 (related to Fig. 1). **Elevated cell lysis in cells lacking PBP1B or CpoB; loss of LpoA exacerbates lysis in the absence of CpoB. A.** Increased cell-envelope lysis or permeability measured by a CPRG assay (Paradis-Bleau *et al.*, 2014) at different salt concentrations. The colorless, LacZ substrate CPRG cannot enter intact cells, where it would yield red CPR, unless the envelope is severely compromised or the cells lyse. Assay was performed on agar plates, on which mutants were arrayed robotically in a 384-colony format (Paradis-Bleau *et al.*, 2014). Box plots of rate of accumulation of CPR color are shown ($n>32$); rates are more sensitive and robust compared to end-point measurements. Box corresponds to 25-75% (IQR). Both $\Delta mrcB$ and $\Delta cpoB$ mutants exhibit elevated cell lysis, but the effect is not additive. As the double $\Delta mrcB \Delta cpoB$ mutant phenocopies the single $\Delta mrcB$ mutant, we deduce that PBP1B is epistatic to CpoB. In contrast, CpoB and LpoA appear to work in redundant pathways, as the double $\Delta lpoA \Delta cpoB$ mutant exhibits much stronger cell lysis than any of the parental mutants. **B.** A $\Delta lpoA \Delta cpoB$ mutant exhibits periplasmic leakage and lysis during growth. Immunodetection of periplasmic (mCherry_{peri}, α -mCherry) and cytoplasmic (RNA polymerase β' subunit, α -RNAP β' ; GroEL) cell contents in filtered culture supernatants (sup) versus pelleted cells (pel); presence of mCherry in sup indicates periplasmic leakage; presence of RNAP β' and GroEL in sup indicates lysis.

Supplemental Figure S2 (related to Fig. 1). **LpoA encodes a second function, and the LpoA TPR domain is dispensable for PBP1A activation. A-B.** Quantification of growth fitness for indicated

1260 mutant strains (see Fig. 1F). **A.** A strain lacking CpoB and LpoA exhibited a synthetic growth defect, but
1261 a strain lacking CpoB and PBP1A (encoded by *mrcA*) did not. A triple $\Delta cpoB \Delta lpoA \Delta mrcA$ mutant also
1262 showed a growth defect, indicating that the growth defect of the $\Delta cpoB \Delta lpoA$ double mutant is not
1263 caused by PBP1A malfunction. **B.** The LpoA TPR domain is dispensable for PBP1A activation. Lack of
1264 PBP1B (encoded by *mrcB*) and LpoA is synthetic lethal because PBP1A requires activation by LpoA;
1265 however a strain lacking PBP1B and the LpoA TPR domain shows no fitness defect. **C.** Summary of
1266 genetic relationships.

1267

1268 **Supplemental Figure S3** (related to Fig. 1). **The N-terminal TPR domain of LpoA encodes a novel**
1269 **function that compensates for loss of CpoB.** **A.** Structure of LpoA (Jean *et al.*, 2014) and summary
1270 of domain functions. The C-terminal domain is required for PBP1A activation; the N-terminal TPR
1271 domain is dispensable for PBP1A activation (Fig. S2B) but required for a second, CpoB-related function.
1272 **B-C.** Quantification of microscopy phenotypes (see Fig. 1D-E). **B.** OM blebbing. **C.** Loss of periplasmic
1273 fluorescence, indicative of periplasmic leakage. **D.** Quantification of growth fitness for indicated mutant
1274 strains (see Fig. 1F). CpoB/compensatory function: +, strains that possess either CpoB, the
1275 compensatory function of the LpoA TPR domain, or both; -, strains that lack both. PBP1A function: +,
1276 strains that possess both PBP1A and the LpoA C-terminal domain, which is required for PBP1A
1277 activation *in vivo*; -, strains that lack one or both. A $\Delta cpoB \Delta mrcA lpoA(\Delta TPR)$ triple mutant lacks both

1278 CpoB/compensatory function and PBP1A function, and thus recapitulates the envelope and growth
1279 defects of the $\Delta cpoB \Delta poA$ mutant.

1280

1281 **Supplemental Figure S4** (related to Fig. 3). **Endogenously-encoded CpoB-mCherry and GFP-TolA**
1282 **fusion proteins are functional. A-B.** Quantification of growth fitness for indicated strains (see Fig. 1B
1283 & 1F). The native chromosomal copy of *cpoB* was replaced with *cpoB-mCherry* to allow endogenous
1284 expression of the mCherry fusion. A $\Delta cpoB \Delta poA$ strain exhibits a severe growth defect, whereas a
1285 *cpoB-mCherry \Delta poA* strain shows no defect, indicating that the CpoB-mCherry fusion is functional. **B.**
1286 The native chromosomal copy of *tolA* was replaced with *gfpmut2-tolA* to allow endogenous expression
1287 of the GFP fusion. A $\Delta tolA$ strain was extremely sensitive to 0.5% SDS and 0.5 mM EDTA (envelope
1288 stress), while the *gfp-tolA* strain showed no defect, indicating that the GFP-TolA fusion is functional.

1289

1290 **Supplemental Figure S5** (related to Fig. 3). **CpoB localizes to mid-cell. A.** WT cells immunolabeled
1291 with antibody to CpoB. **B.** Average distribution of CpoB along the length of the cell (see Fig. 3C). **C.**
1292 Localization of CpoB as a function of cell cycle progression (see Fig. 3B). **D.** Antibody to CpoB is
1293 specific. Image and profile map of $\Delta cpoB$ cells immunolabeled with antibody to CpoB; no appreciable
1294 fluorescence signal is observed.

1295

1296 **Supplemental Figure S6** (related to Fig. 3). **Timing of localization to mid-cell for CpoB-mCherry,**
1297 **GFP-TolA, and PBP1B, with comparison to divisome proteins FtsZ, PBP3, and FtsN. A.** Average
1298 distribution of indicated cell division proteins for different cell-cycle progression age groups (see Fig. 3C
1299 and key, bottom-right). Profiles of the 10 age classes for each protein have been offset equally to
1300 facilitate comparison and minimize overlap. Each age group contains 300-500 cells. *, age class when
1301 increased localization at mid-cell was first observed. **B.** Localization summary table. ¹Ring fraction, the
1302 amount of mid-cell fluorescence in a rectangle of 0.8 μ m divided by the total fluorescence in the cell at
1303 the time point corresponding to the moment. ²Initiation, the time point in the division cycle where the
1304 fluorescence at mid cell starts to increase as determined from the collective profiles in age classes of
1305 10% (Fig. S6A). ³Moment, the time point in the cell cycle when mid-cell fluorescence is highest. ⁴Data
1306 from (van der Ploeg *et al.*, 2013). *, CpoB-mCherry was used instead of immunolabeling so as to allow
1307 live-cell imaging; we have found that freely diffusing periplasmic proteins do not retain their original
1308 localization following fixation, likely due to osmotic effects. **, GFP-TolA was used because the quality
1309 of available TolA antiserum was not sufficient for reliable labeling.

1310

1311 **Supplemental Figure S7** (related to Fig. 3). **Localization of CpoB to mid-cell is dependent on**
1312 **divisome assembly and function. A-G.** Profile maps showing localization of CpoB as a function of
1313 cell cycle progression (see Fig. 3B), visualized by immunolabeling cells of the indicated strains with
1314 antibody specific to CpoB. **A-E.** For wild type and temperature-sensitive (ts) strains, localization at both

the permissive (28°C, left) and restrictive (42°C, right) temperatures is shown. **A.** Parental wild type strain (LMC500). **B.** FtsZ(ts) strain LMC509 is not completely temperature sensitive; consequently, CpoB still localizes at mid-cell in shorter pre-divisional cells, but not in longer smooth filaments. **E.** PBP3(ts) strain LMC510 is already somewhat elongated at the permissive temperature because even at this temperature the PBP3(ts) protein is partially unstable (Fraipont *et al.*, 2011). **F.** CpoB localization over the course of FtsN depletion (see Methods). **G.** CpoB localization following treatment with aztreonam, which inhibits PG synthesis by PBP3. CpoB localization to mid-cell is thus dependent on FtsZ, FtsA, FtsW, PBP3, ongoing PBP3-mediated PG synthesis, and FtsN.

1323

Supplemental Figure S8 (related to Fig. 3). **Localization of CpoB to mid-cell is independent of PBP1B and TolA.** **A-B.** Profile maps showing localization of CpoB as a function of cell-cycle progression (see Fig. 3B), visualized by immunolabeling cells of the indicated strains. Cell width (diameter) is based on phase contrast images; darkening indicates constriction at mid-cell. **A.** CpoB localizes to mid-cell in the absence of PBP1B (encoded by *mrcB*). **B.** CpoB localizes to mid-cell in the absence of TolA. Loss of TolA causes mild cell chaining, observed here in the longer $\Delta tolA$ cells possessing multiple points of constriction ($\Delta tolA$, cell width plot). CpoB also localizes to these future division sites. Cells were grown under conditions that minimized non-specific accumulation of periplasmic proteins at the septum in $\Delta tolA$ cells (glucose minimal medium (GB1) pH 7.0, 28°C; see Methods).

1334

1335 **Supplemental Figure S9** (related to Fig. 4). **Demonstration of ternary complexes *in vitro*. A.**

1336 Ternary complexes of LpoB-PBP1B-CpoB and LpoB-PBP1B-TolA detected by *in vitro* cross-linking/pull-
1337 down. Proteins were cross-linked and applied to Ni-NTA beads. Cross-linkage of bound proteins was
1338 cleaved and samples separated by SDS-PAGE. His-LpoB retained CpoB or TolA only in the presence
1339 of PBP1B, indicating the presence of His-LpoB-PBP1B-CpoB and His-LpoB-PBP1B-TolA complexes.
1340 In the presence of PBP1B, His-LpoB also simultaneously retained CpoB and TolA, suggesting a
1341 tetrameric complex. **B.** Ternary complex of PBP1B, CpoB and TolA. Mixtures of proteins (indicated
1342 above) were cross-linked and complexes were resolved by SDS-PAGE. After Western blot PBP1B,
1343 CpoB and TolA were detected by specific antibodies. The CpoB-TolA complex (blue box) and several
1344 bands containing all three proteins (green, orange and red boxes) were detected. The bottom part
1345 shows an experiment where PBP1B was replaced by PBP1A, showing the absence of the ternary
1346 complex bands.

1347

1348 **Supplemental Figure S10** (related to Fig. 4). **CpoB copy number determination.**

1349 Representative western blot detection of CpoB from BW25113 whole cell lysate along with purified
1350 CpoB standards. Standards were loaded in BW25113 $\Delta cpoB$ lysate to ensure a similar transfer
1351 efficiency to the endogenous CpoB. Chemiluminescence signal was quantified using the ImageQuant
1352 LAS4000 software.

1353

1354 **Supplemental Figure S11** (related to Fig. 5). **PBP1B GTase and TPase activity assays. A.** PBP1B
1355 GTase activity assay. Representative continuous fluorescence assay graphs for GTase data shown in
1356 Fig. 5. PBP1B concentrations were 0.5 μ M (graphs 2 and 4) or 1 μ M (graphs 1 and 3), the differences
1357 in basal PBP1B activity are also due to different detergent concentration in the reactions. The reactions
1358 shown in the bottom graph were performed at a lower temperature of 25°C to slow the reaction and
1359 allow the measurement of initial rates. Proteins present in each reaction are indicated next to their
1360 corresponding curves in the same colour. Each point is the mean \pm SD of three or four independent
1361 experiments. **B.** PBP1B TPase activity assay. Representative examples of HPLC chromatograms for
1362 TPase data shown in Fig. 5B. PBP1B was incubated with radioactive lipid II and 150 mM NaCl
1363 (standard condition, top chromatograms) or 215 mM NaCl (bottom chromatograms) in the presence of
1364 the proteins indicated above the corresponding chromatogram. The resulting PG was digested with
1365 muramidase (cellosyl) yielding muropeptides, which were reduced with sodium borohydride and
1366 separated by HPLC. The percentage of peptides in cross-links was calculated as 100% - the
1367 monomeric (non-cross-linked) disaccharide pentapeptide (peak 1). Peak 2 corresponds to bis-
1368 disaccharide tetrapentapeptide, and peak 3 to tris-disaccharide tetratetrapentapeptide.

1369

1370 **Table 1. His6-PBP1B pBpa - CpoB cross-linking mass spectroscopy data**

1371

mutant	score ^a	coverage ^b	peptides ^c	PSM ^d
T118	300.52	19.77%	7	12
E123	79.99	11.41%	3	4
T751	79.99	11.41%	3	4
T753	301.64	19.77%	7	12

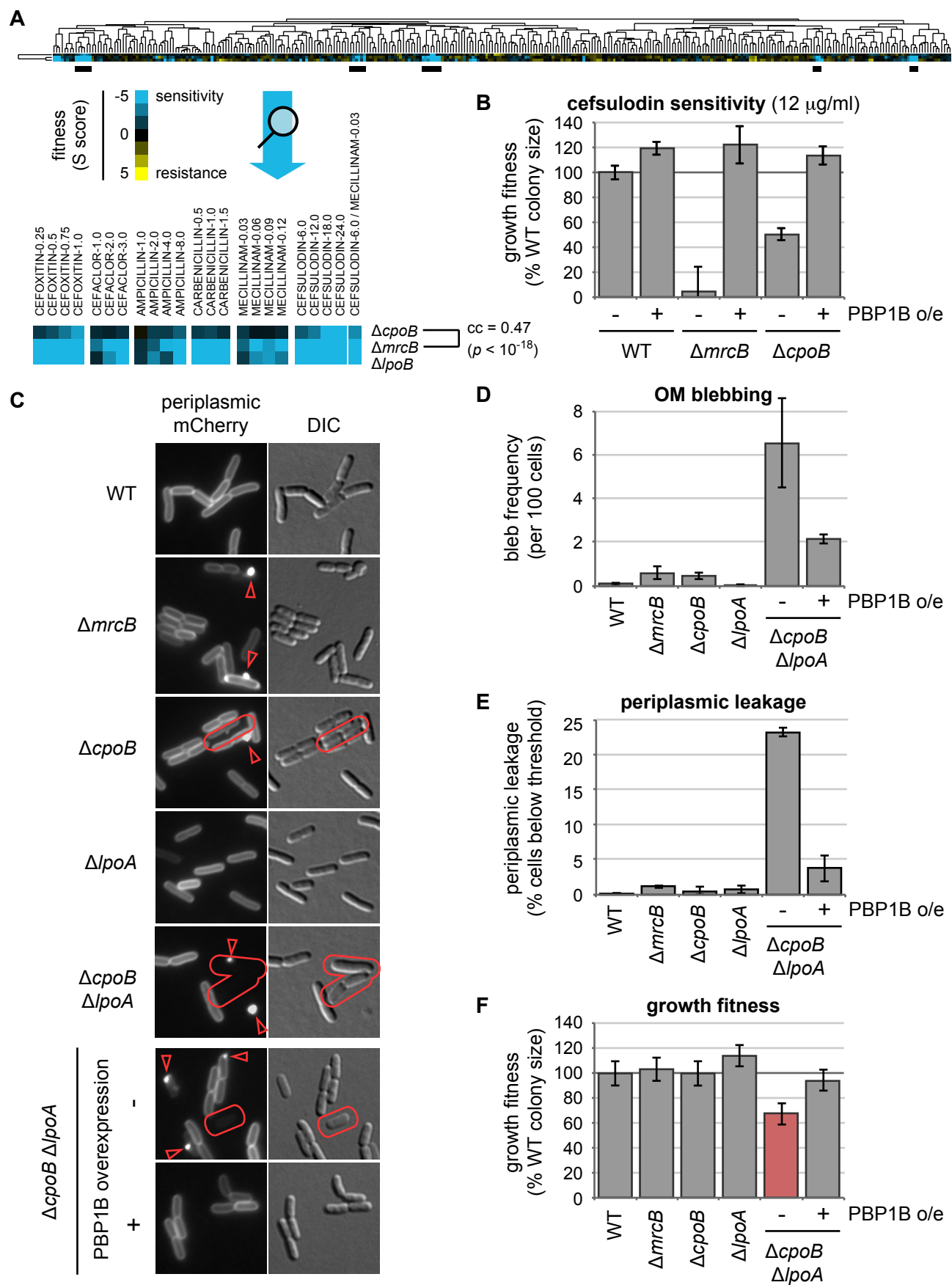
1372

1373 ^a addition of individual scores of the ion fragmentation spectra of the identified peptides

1374 ^b percentage of protein sequence covered by the identified peptides

1375 ^c number of unique peptides of the protein identified in the sample

1376 ^d number of individual spectra in which the peptides were identified



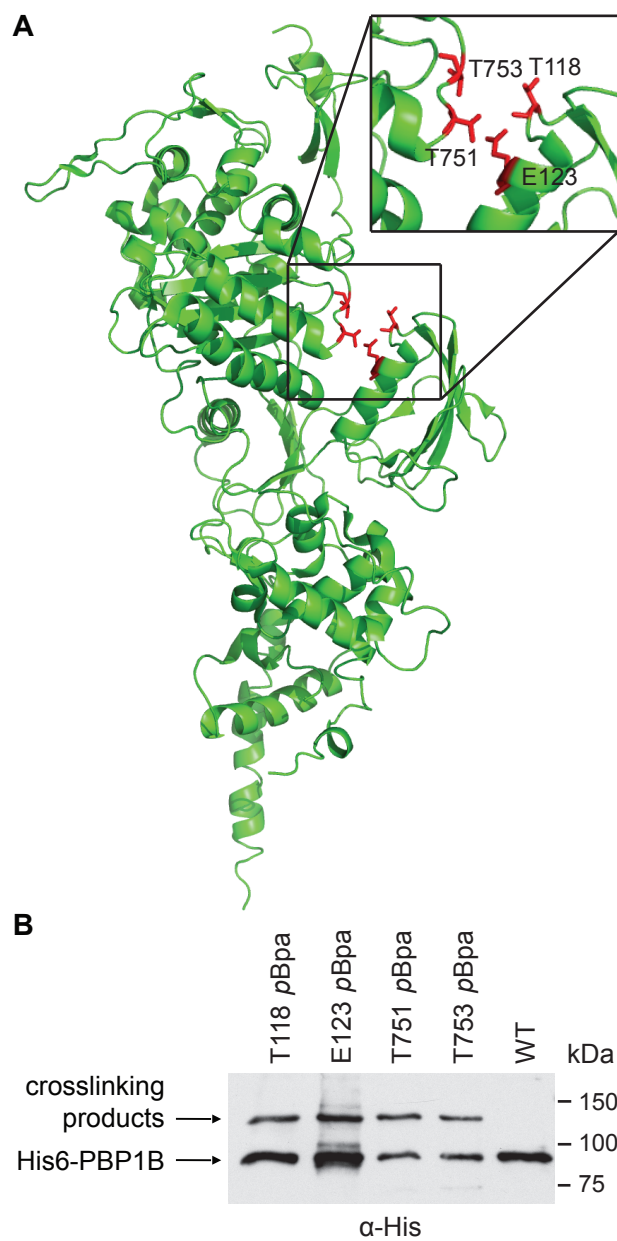


Figure 2. PBP1B interacts with CpoB *in vivo*.

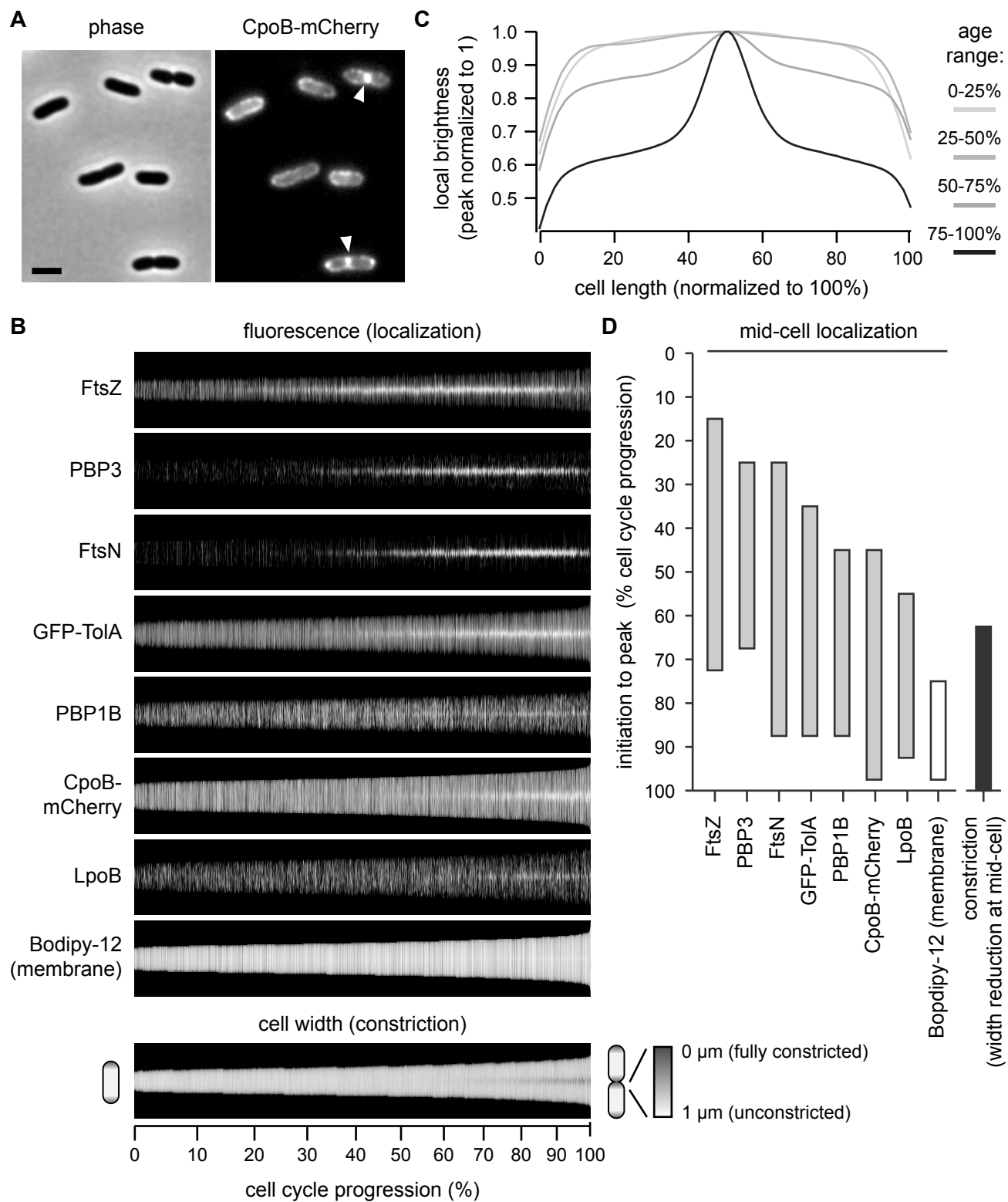


Figure 3. CpoB localizes to mid-cell concurrent with PBP1B, TolA, and the onset of OM constriction.

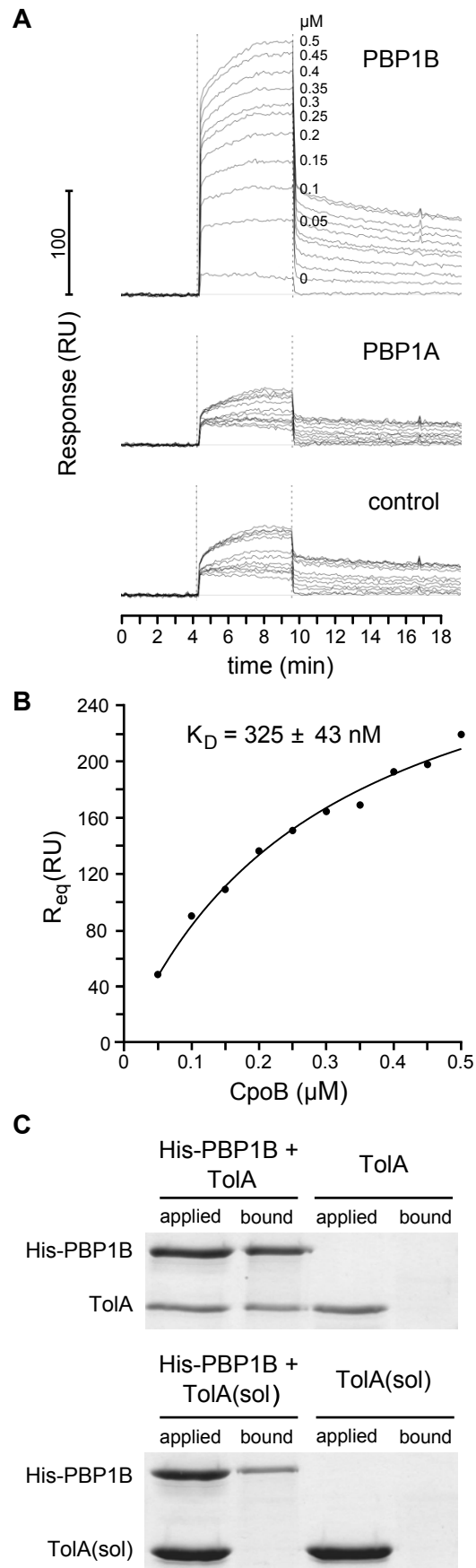


Figure 4. PBP1B interacts directly with CpoB and TolA.

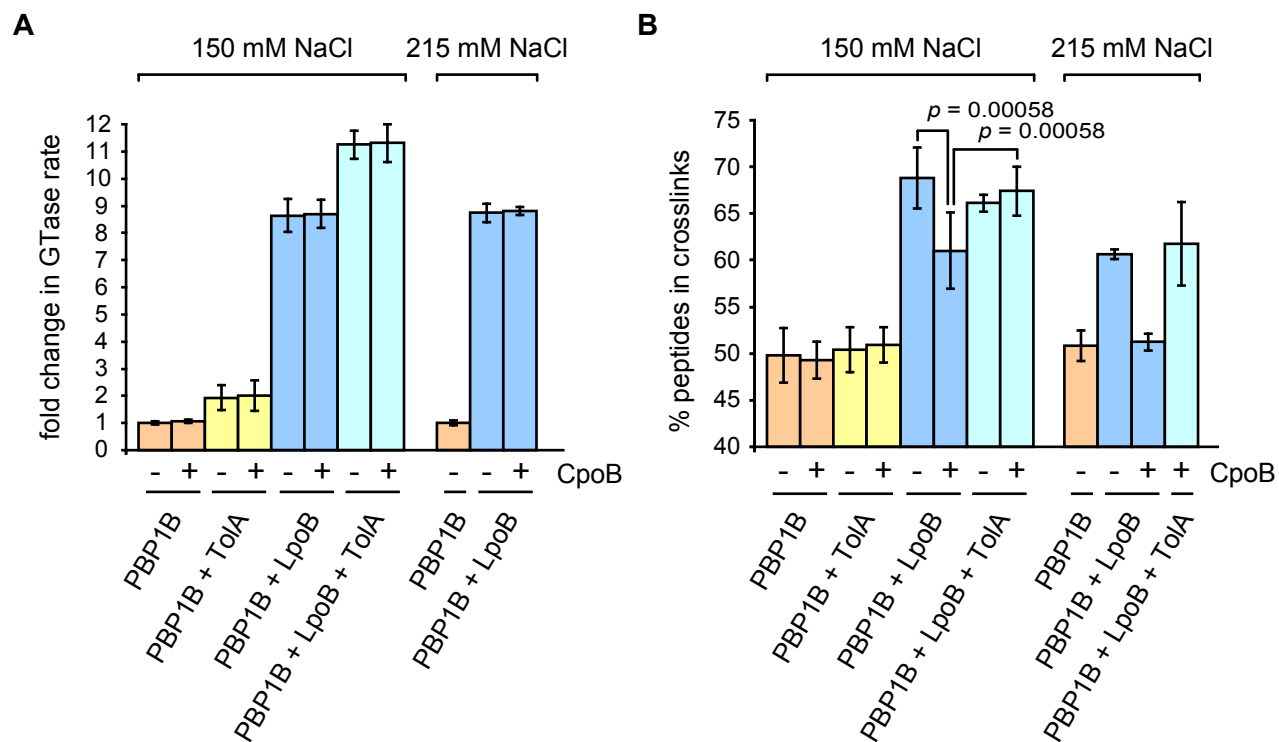


Figure 5. CpoB modulates stimulation of PBP1B TPase activity by LpoB.

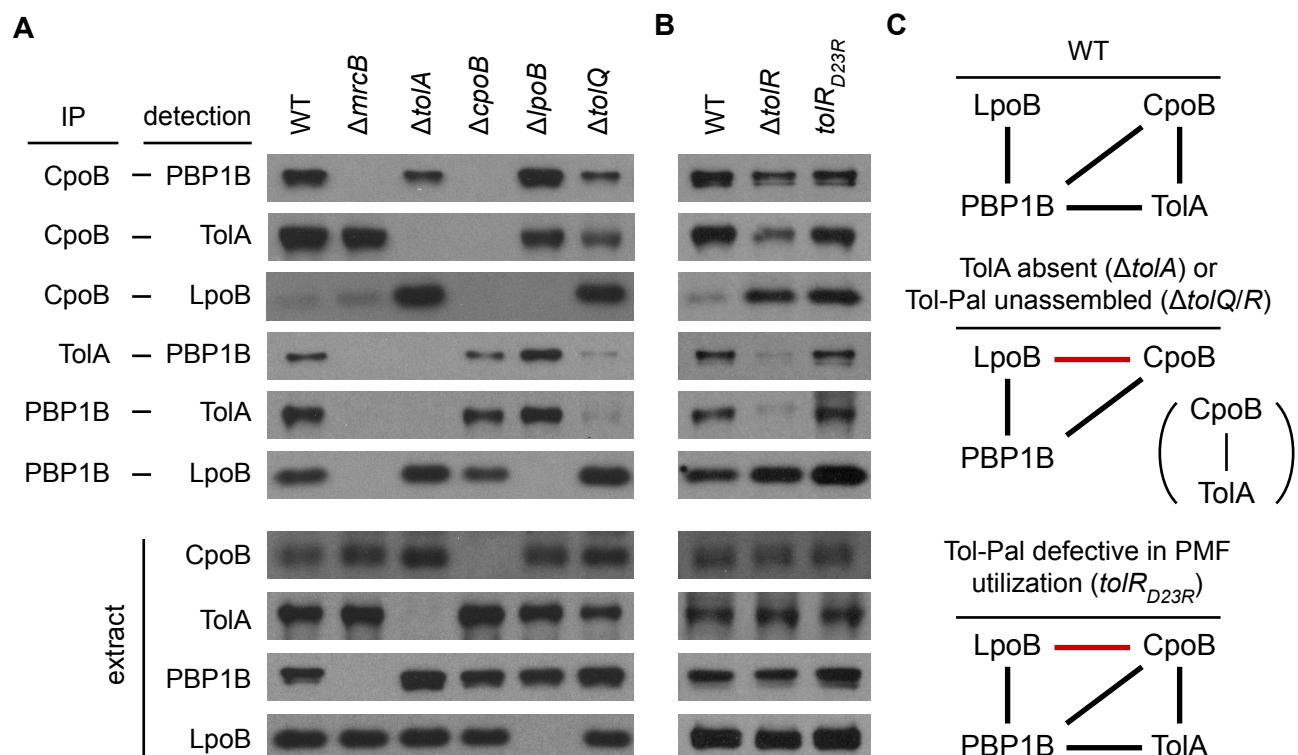


Figure 6. Regulatory interactions between CpoB, TolA, and PBP1B-LpoB respond to Tol-Pal assembly and energy state.

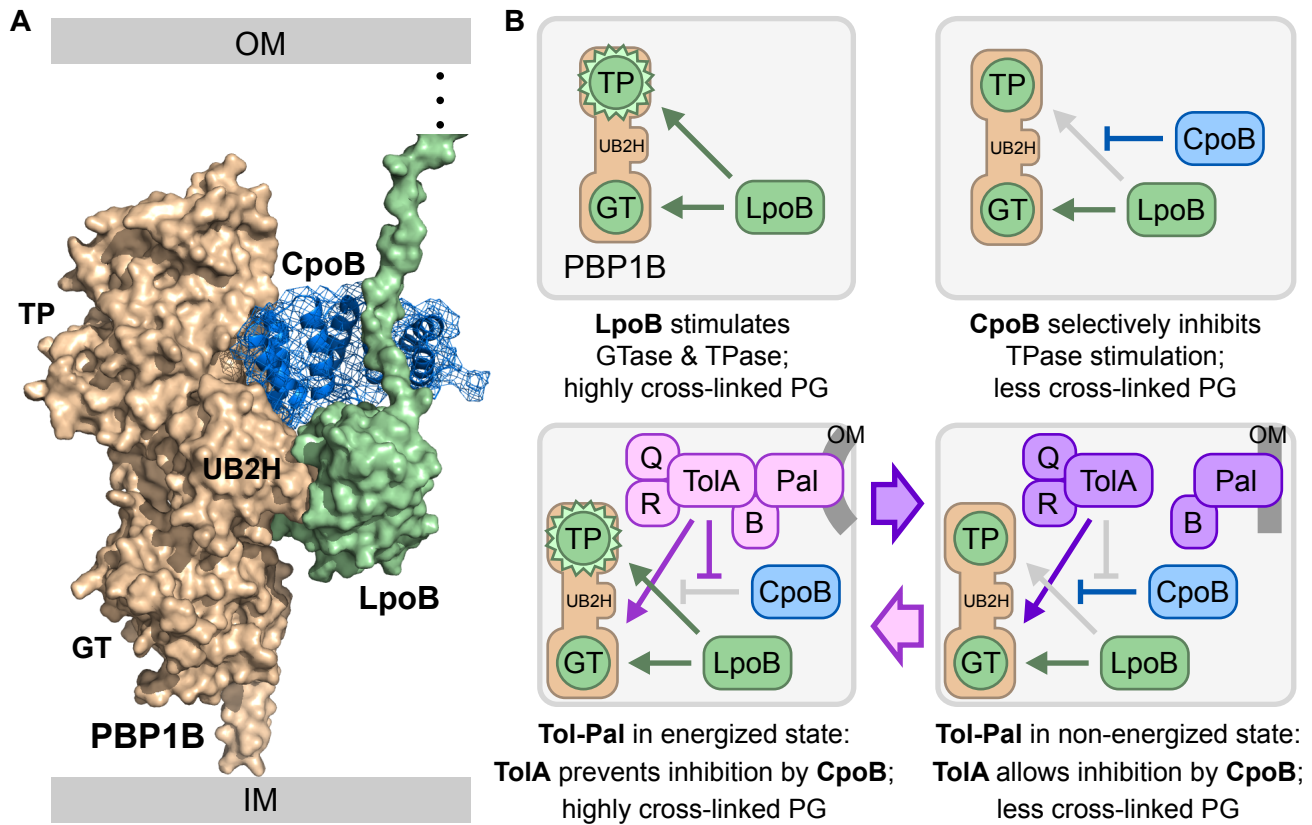
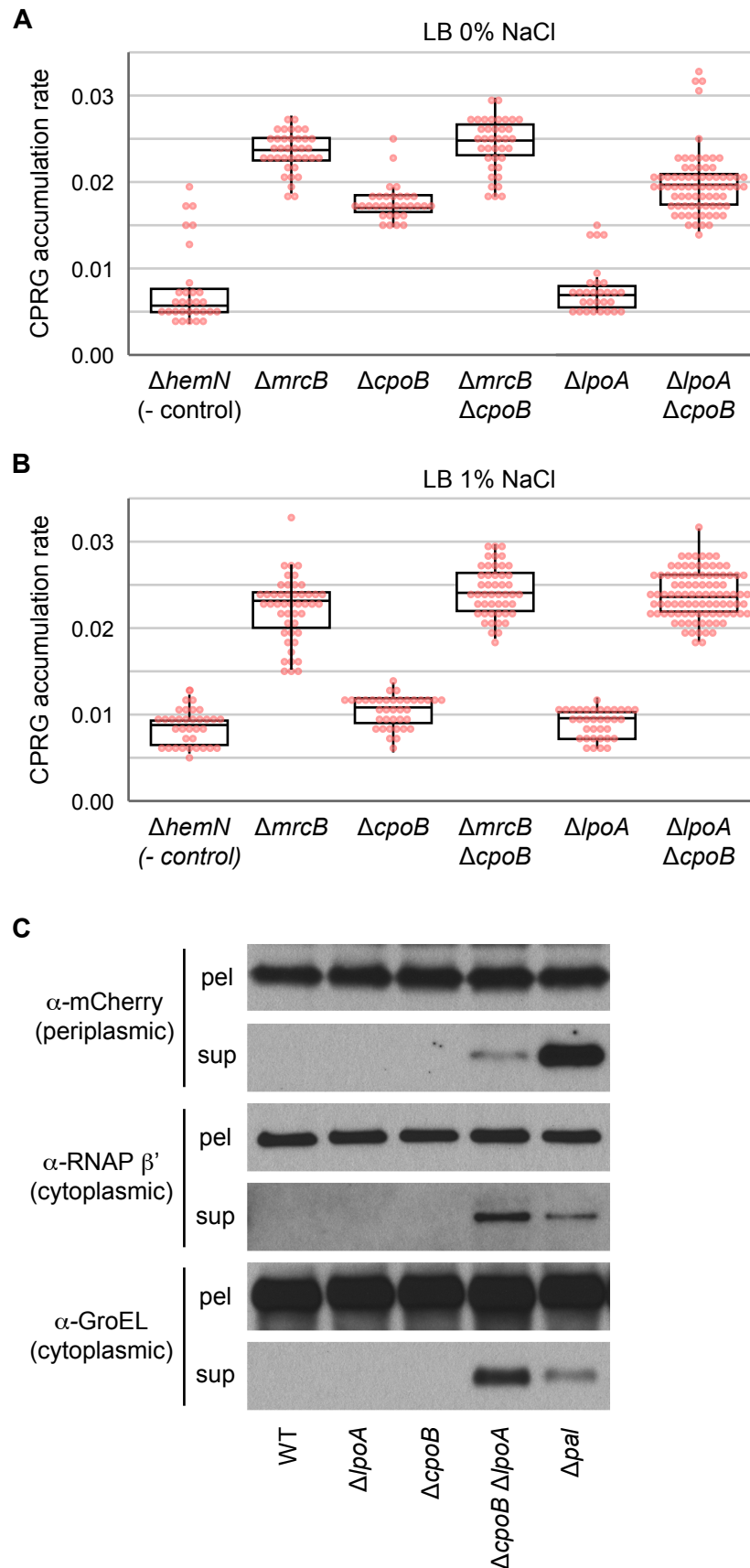
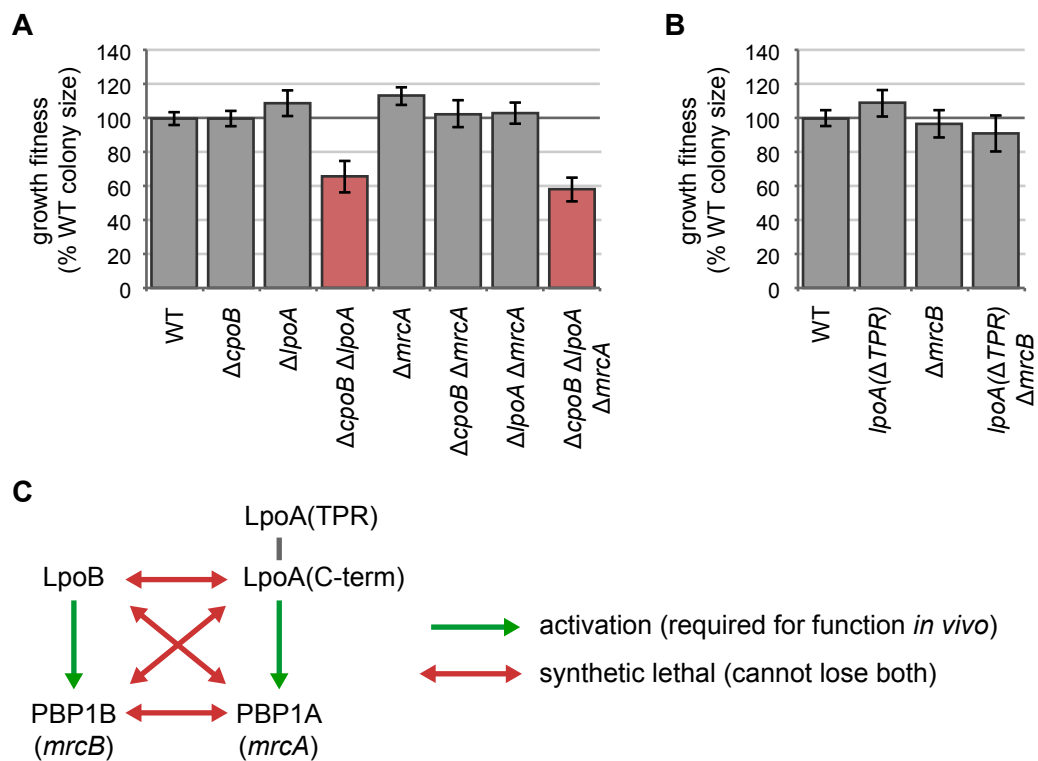


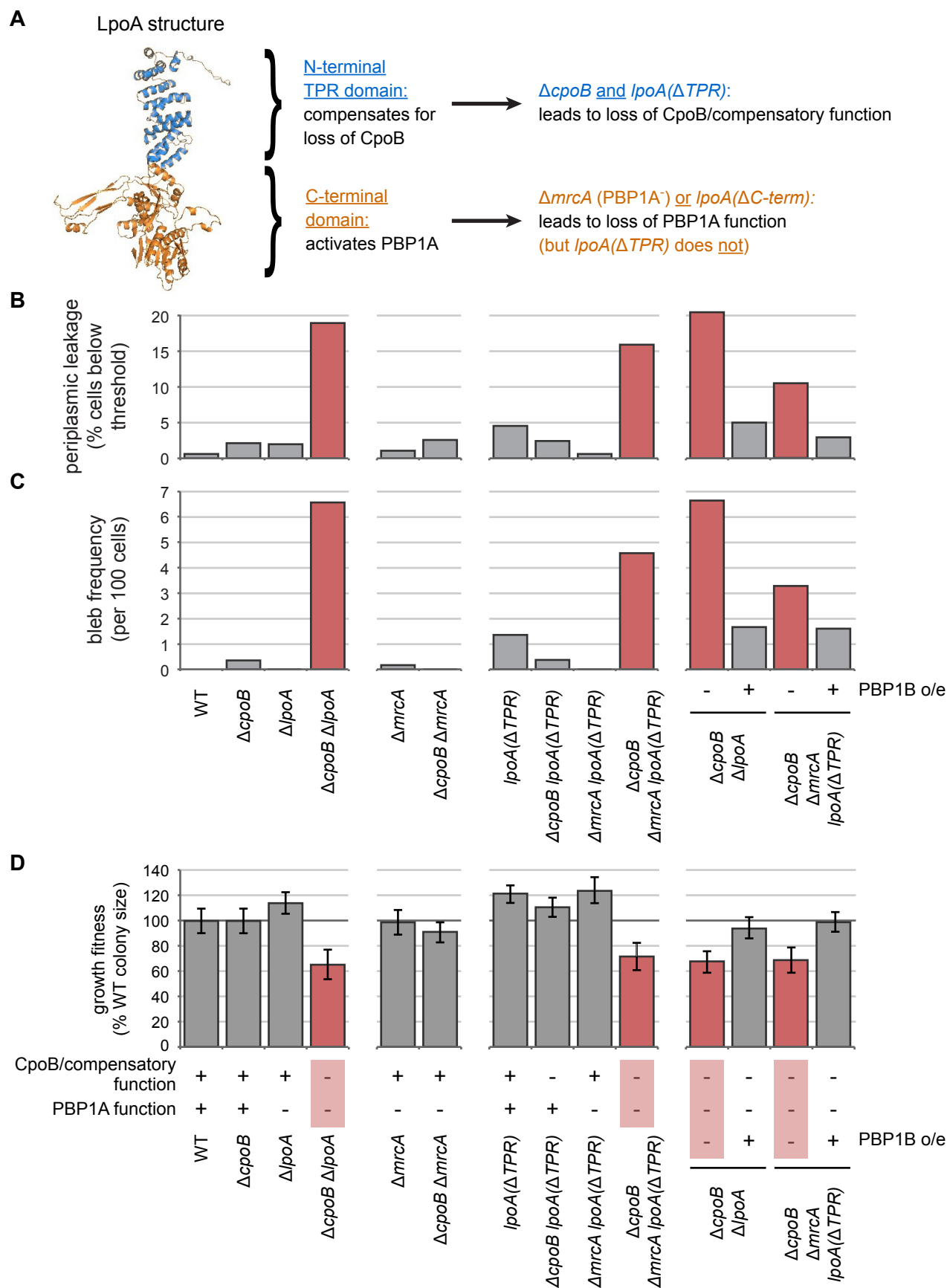
Figure 7. Model for physical and functional coordination of the PBPB-LpoB PG synthesis and Tol-Pal OM constriction machines by CpoB.



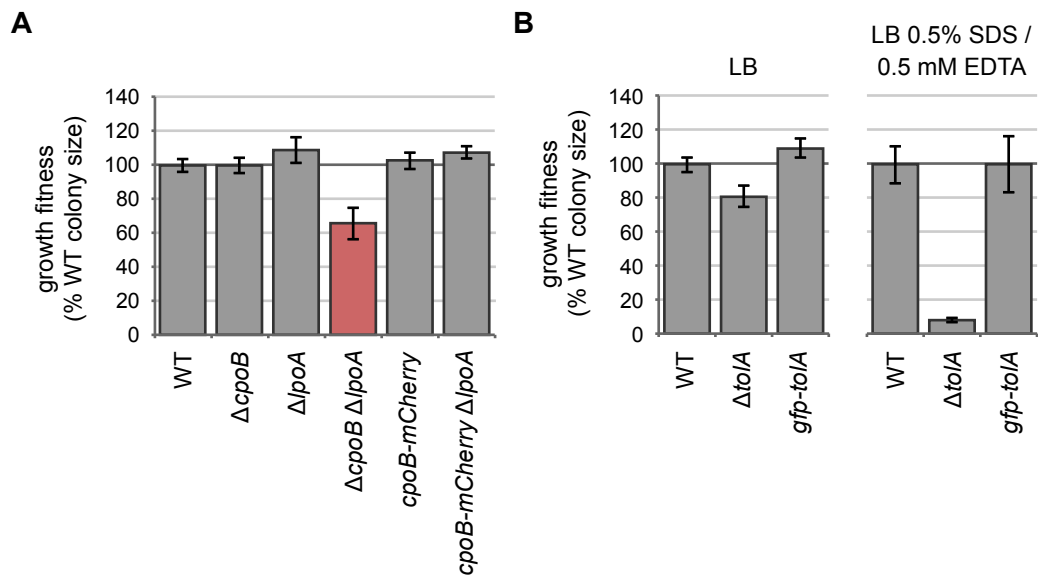
Supplemental Figure S1 (related to Fig. 1). **Elevated cell lysis in cells lacking PBP1B or CpoB; loss of LpoA exacerbates lysis in the absence of CpoB.**



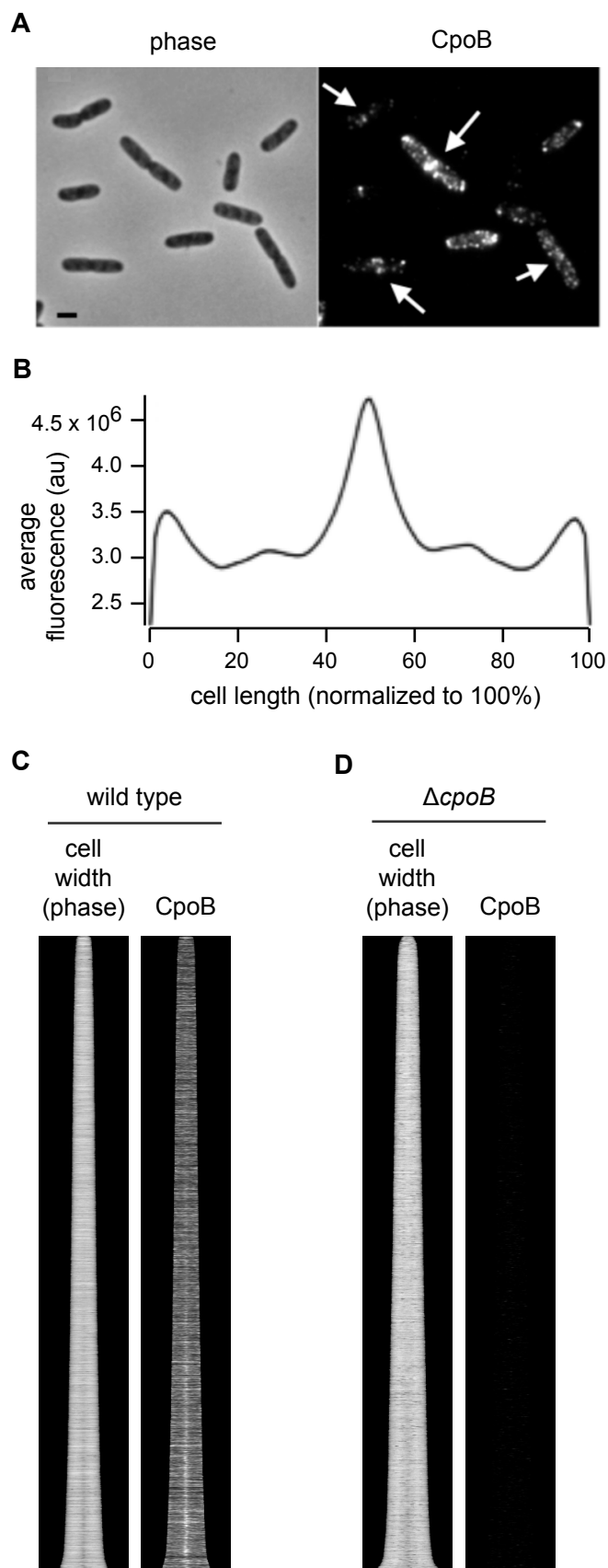
Supplemental Figure S2 (related to Fig. 1). **LpoA encodes a second function, and the LpoA TPR domain is dispensable for PBP1A activation.**



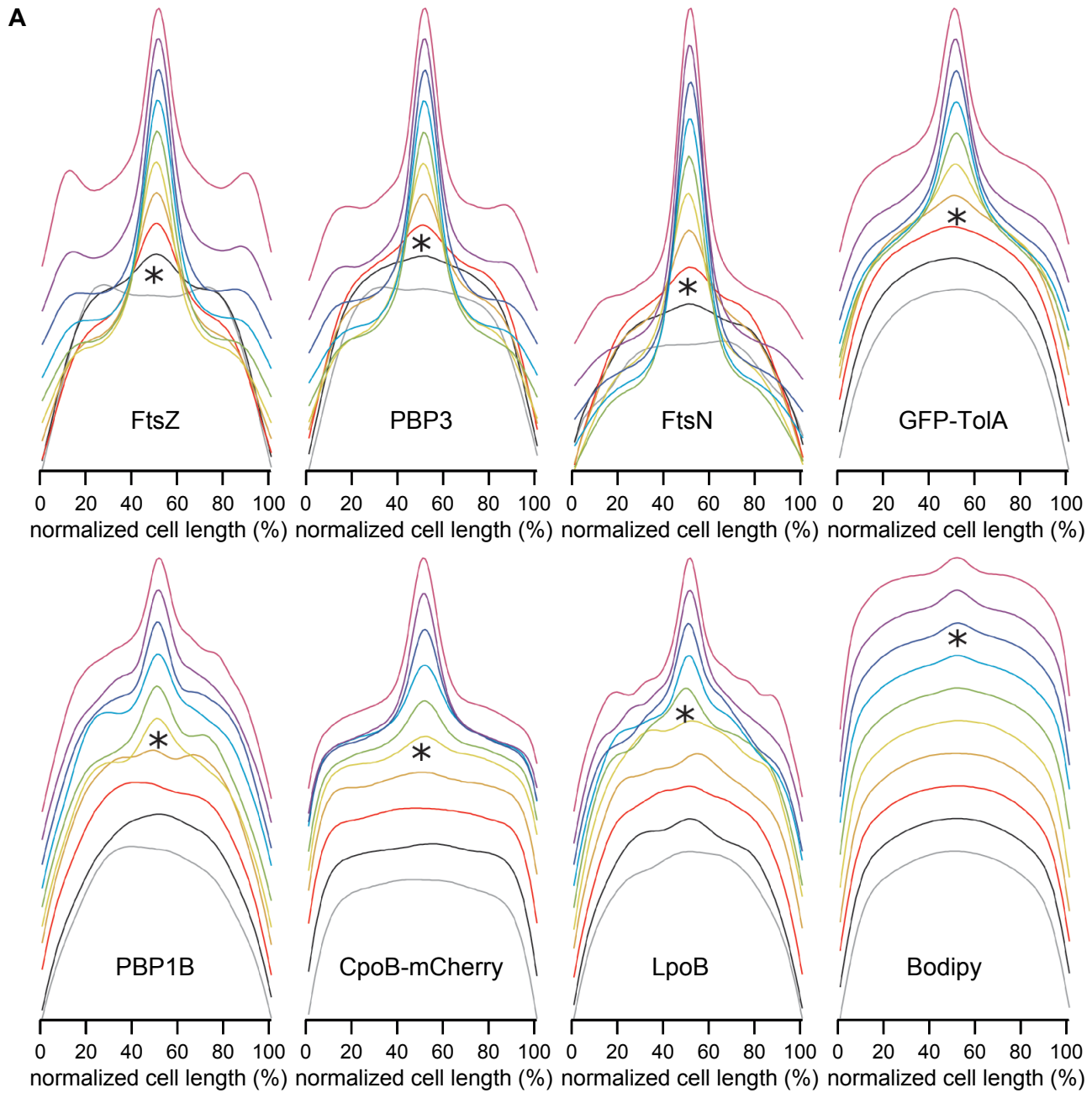
Supplemental Figure S3 (related to Fig. 1). The N-terminal TPR domain of LpoA encodes a novel function that compensates for loss of CpoB.



Supplemental Figure S4 (related to Fig. 3). **Endogenously-encoded CpoB-mCherry and GFP-TolA fusion proteins are functional.**



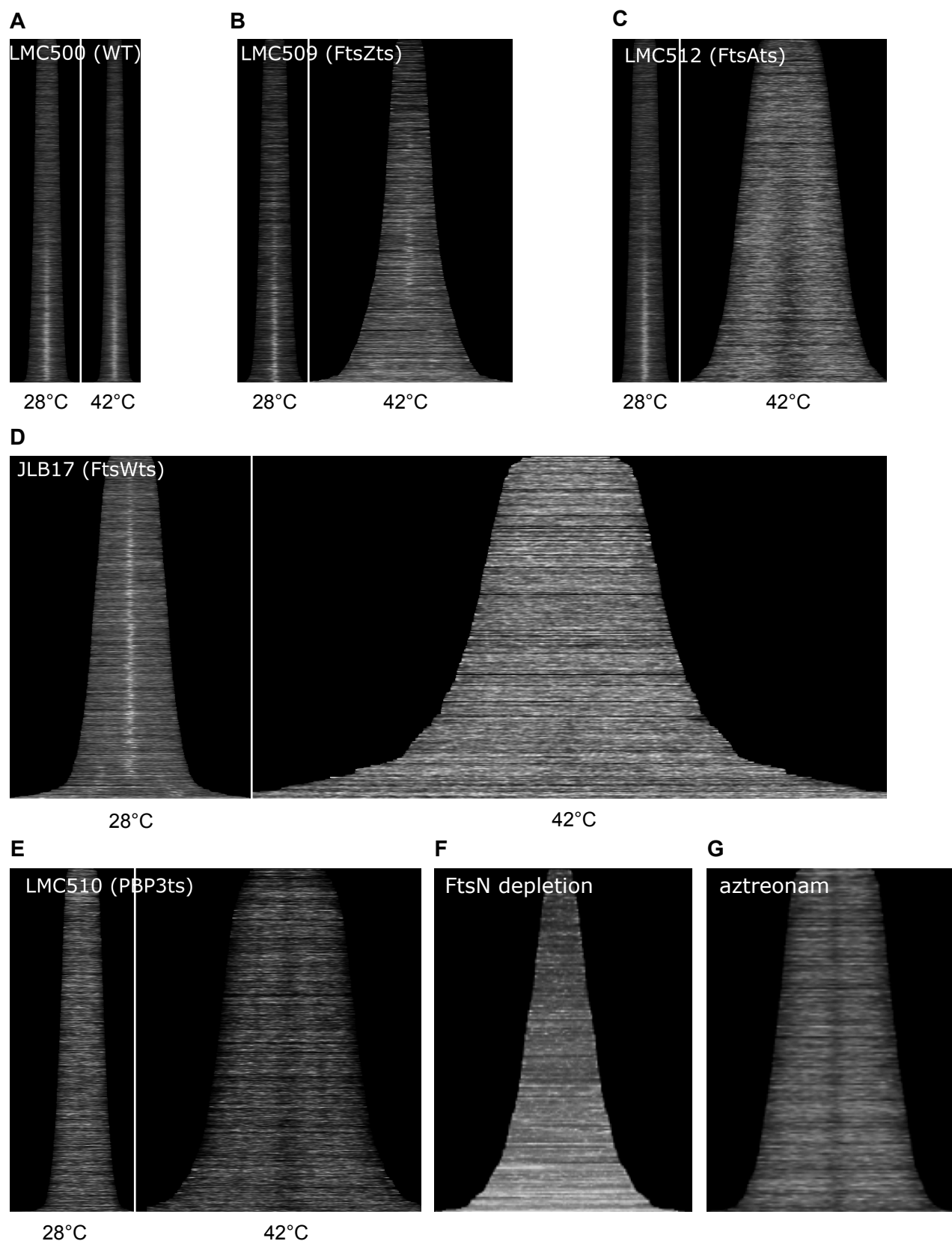
Supplemental Figure S5 (related to Fig. 3). **CpoB localizes to mid-cell.**



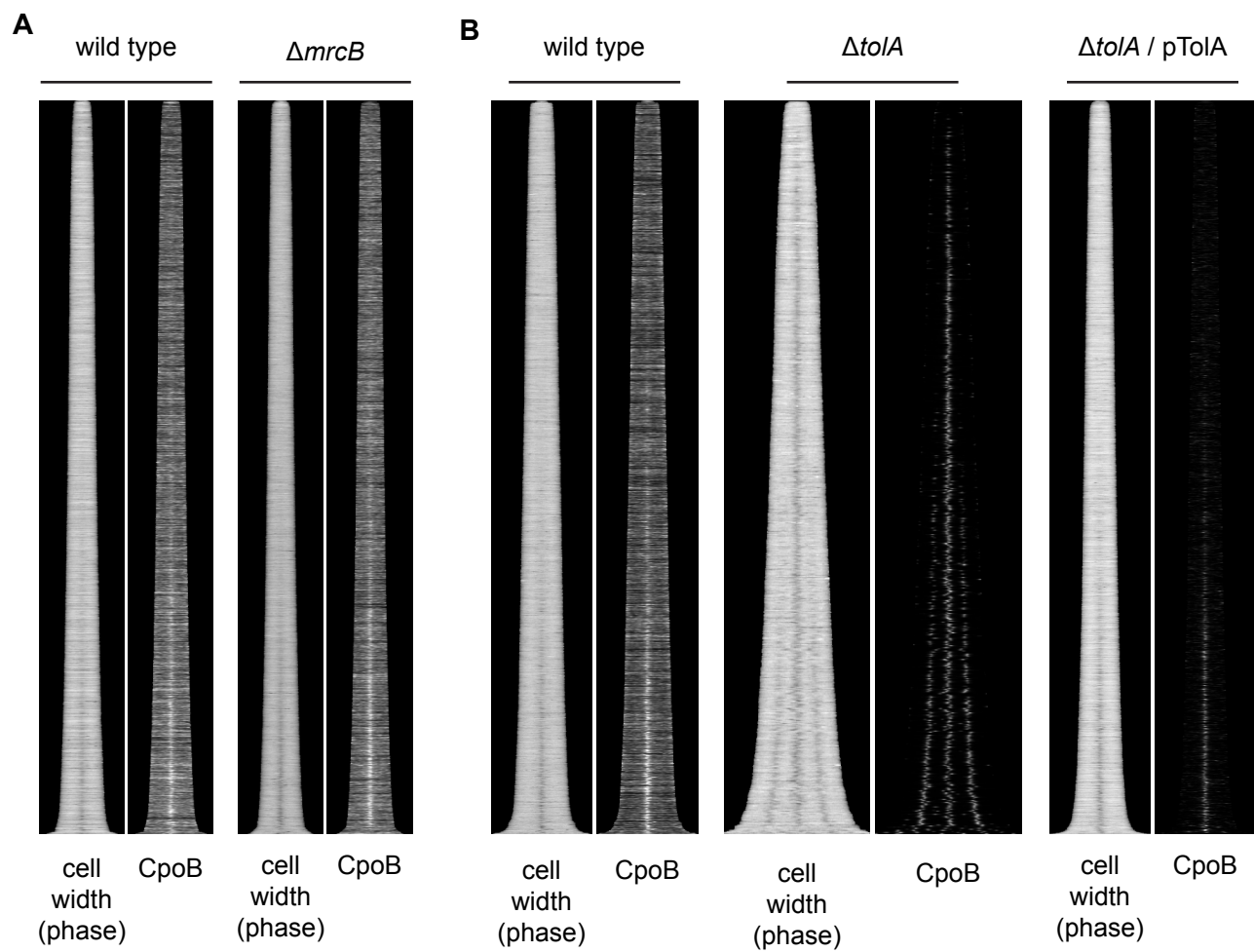
B

Immunolabeled protein	Ring Fraction (%) ¹	Age class initiation (%) ²	Moment (%) ³		
FtsZ ⁴	31.4 ± 1.4	10-20	72.5	— 0-10%	age class key (% cell cycle progression)
PBP3 ⁴	33.0 ± 2.1	20-30	67.5	— 10-20%	
FtsN ⁴	42.0 ± 2.2	20-30	87.5	— 20-30%	
PBP1B	11.7 ± 1.8	40-50	87.5	— 30-40%	
LpoB	11.4 ± 1.6	50-60	92.5	— 40-50%	
CpoB	32.6 ± 2.4	40-50	87.5	— 50-60%	
CpoB-mCherry*	13.3 ± 1.0	40-50	97.5	— 60-70%	
GFP-TolA**	19.0 ± 0.8	30-40	87.5	— 70-80%	
Bodipy	3.75 ± 0.31	70-80	97.5	— 80-90%	
				— 90-100%	

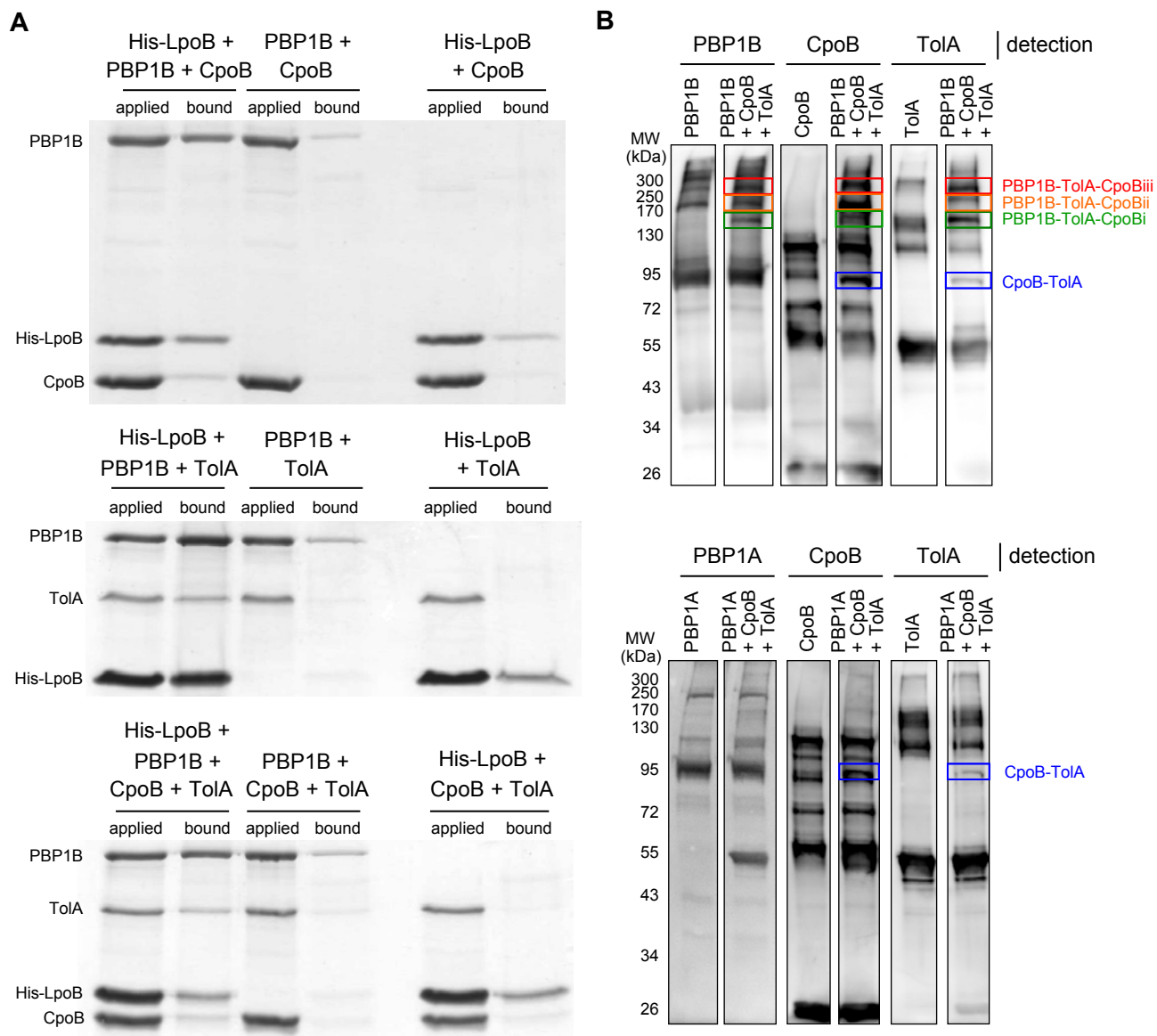
Supplemental Figure S6 (related to Fig. 3). Timing of localization to mid-cell for CpoB-mCherry, GFP-TolA, and PBP1B, with comparison to divisome proteins FtsZ, PBP3, and FtsN.



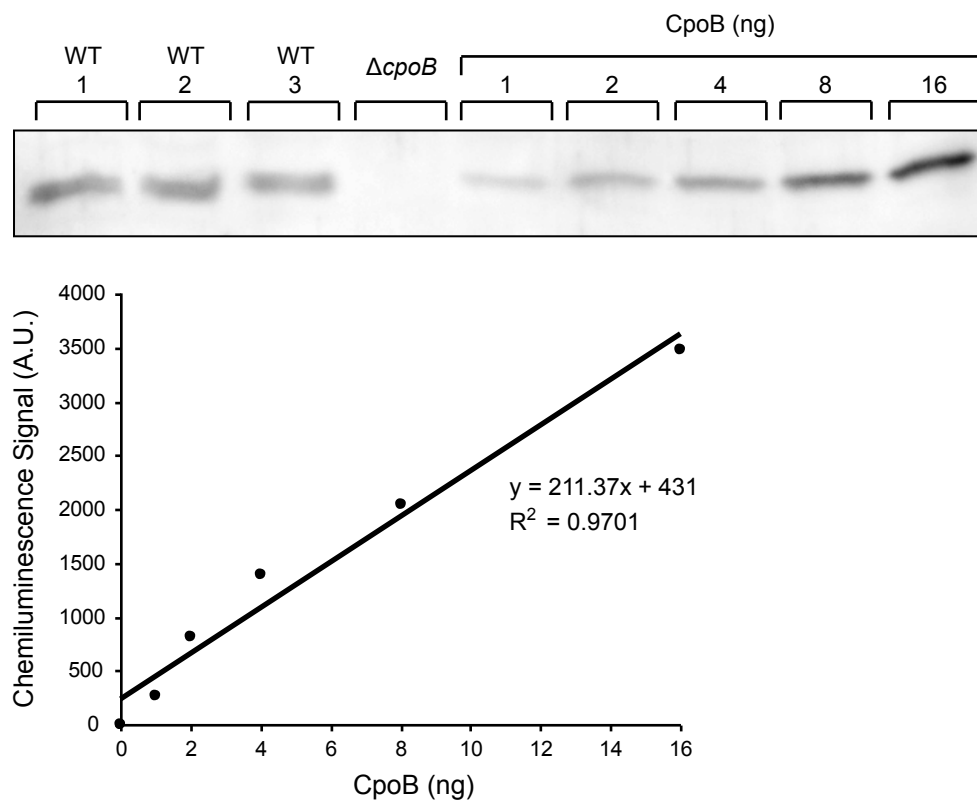
Supplemental Figure S7 (related to Fig. 3). **Localization of CpoB to mid-cell is dependent on divisome assembly and function.**



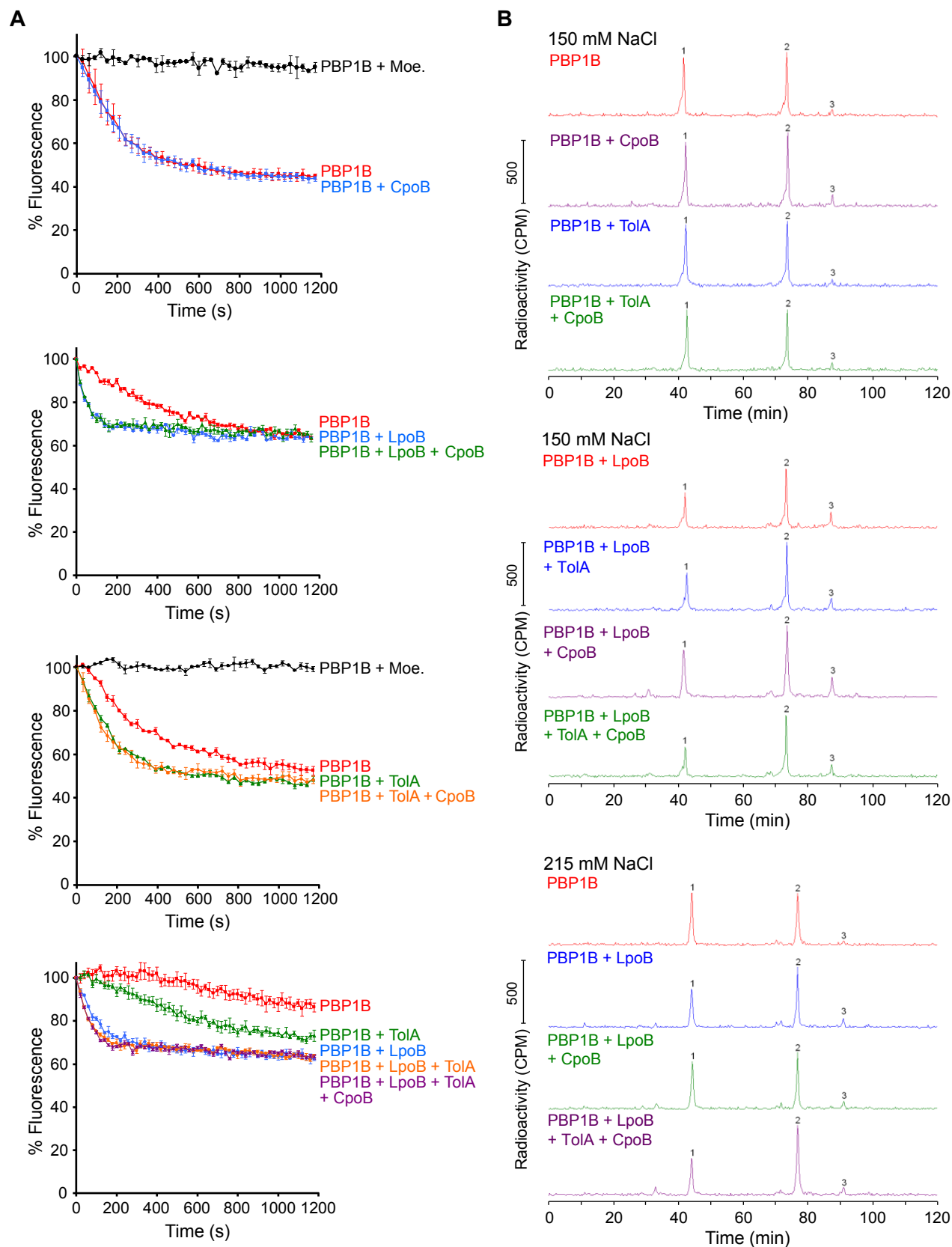
Supplemental Figure S8 (related to Fig. 3). **Localization of CpoB to mid-cell is independent of PBP1B and TolA.**



Supplemental Figure S9 (related to Fig. 4). **Demonstration of ternary complexes *in vitro*.**



Supplemental Figure S10 (related to Fig. 4). **CpoB copy number determination.**



Supplemental Figure S11 (related to Fig. 5). **PBP1B Gase and TPase activity assays.**